Solid State Phenomena
ISSN: 1662-9779, Vol. 300, pp 107-134
doi:10.4028/www.scientific.net/SSP.300.107

Submitted: 2019-04-22
Revised: 2019-07-24
Accepted: 2019-08-08
Online: 2020-02-12

CHAPTER 5

Effect of Water Vapour on the High Temperature Oxidation of Stainless Steels

Somrerk Chandra-ambhorn[1,a], Patthranit Wongpromrat[2,b], Thammaporn Thublaor[1,c] and Walairat Chandra-ambhorn[2,d*]

[1]High Temperature Corrosion Research Centre, Department of Materials and Production Technology Engineering, Faculty of Engineering, King Mongkut's University of Technology North Bangkok, 1518, Pracharat 1 Road, Bangsue, Bangkok, 10800, Thailand

[2]Department of Chemical Engineering, Faculty of Engineering, King Mongkut's Institute of Technology Ladkrabang, Chalongkrung 1 Road, Lat Krabang, Bangkok, 10520, Thailand

[a]somrerk.c@eng.kmutnb.ac.th, [b]patthranit.wo@kmitl.ac.th, [c]thammaporn.tt@gmail.com, [d]walairat.ch@kmitl.ac.th

Keywords: high temperature oxidation, stainless steel, alloying element, chromia, alumina

Abstract. This chapter primarily reviews the nature of water vapour when it presents in bulk gas. The change in a ratio between water vapour and corresponding dissociated hydrogen, which determine the thermodynamic stability of the oxide formation, is analysed when the oxidation kinetics are linear and parabolic. When water vapour reaches the solid/gas interface, chromium species volatilisation and oxidation controlled by surface reaction can occur. The adsorbed water vapour can be further incorporated into the oxide possibly in the form of hydrogen defects. The role of these defects on altering the defect structure of the oxide is discussed. Finally, characteristics of the oxide scale on stainless steels formed in the atmosphere containing water vapour are reviewed.

5.1 Water Vapour in the Bulk Gas

In practice, water vapour presents in various atmospheres such as in ambient air of the industrial processes [1–4] or in atmospheres on cathode or anode sides of solid oxide fuel cells [5–7]. The presence of water vapour could significantly change the oxidation rate and behaviour of the metals. In the classic 2001 paper titled "The kinetic behaviour of metals in water vapour at high temperature: Can general rules be proposed?", Galerie et al. summarised that "water vapour may react more rapidly with metals than oxygen provided that the formed oxide can grow by transport of hydroxyl ion. If such a transport is not possible, the rate of the reaction will depend on the surface acidity of the oxide: less acidic is the oxide, slower is the reaction." [8]. From the time of that publication, the extensive research on water vapour effect on stainless steel oxidation has been conducted under his guidance. A part of those works is reviewed here together with the other ones relevant to this topic. The chapter starts from the analysis of water vapour in the bulk gas. It is then followed by the situations when water vapour arrives at the scale/gas interface and when the adsorbed water is incorporated into the oxide scale in the form of hydrogen defect.

As for the water vapour in the bulk gas, when water vapour presents in the atmosphere, it can dissociate giving H_2 and O_2 according to the following global reaction:

$$H_2O \leftrightarrow H_2 + \frac{1}{2}O_2 \tag{5.1}$$

with

$$\mathrm{K_w} = \exp\left(\frac{-\Delta G_{\mathrm{w}}^{\circ}}{\mathrm{R}T}\right) = \frac{p_{\mathrm{H_2}} p_{\mathrm{O_2}}^{1/2}}{p_{\mathrm{H_2O}}} \tag{5.2}$$

$\mathrm{K_w}$ and $\Delta G_{\mathrm{w}}^{\circ}$ are the equilibrium constant and standard Gibbs free energy of water dissociation reaction as Reaction 5.1, respectively. If the bulk gas contains water vapour mixed with an inert gas, the values of the equilibrium partial pressure of oxygen, $(p_{\mathrm{O_2}})_{\mathrm{eq}}$, dissociated from Reaction 5.1 can be calculated as explained in Section 3.2. Fig. 5.1 shows the temperature-dependent equilibrium partial pressure of oxygen dissociated from water vapour and from the Ar-H_2O gas mixture. It can be used to identify the equilibrium oxygen partial pressure in Ar-H_2O when the water vapour content in the atmosphere is varied.

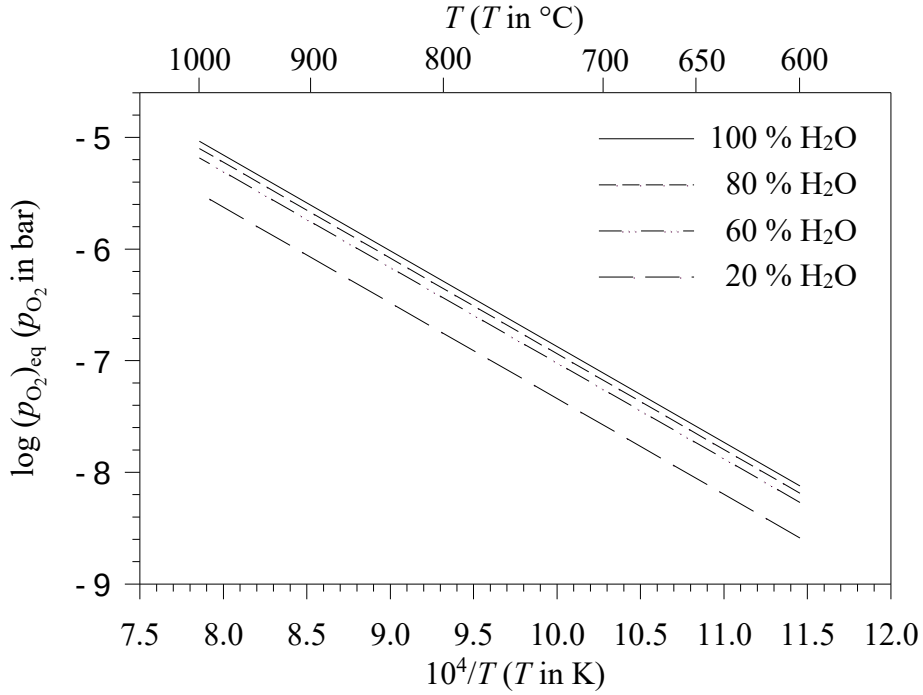

Fig. 5.1. Equilibrium partial pressure of oxygen in Ar-20% H_2O gas mixture constructed using thermodynamic data from Kubaschewski et al. [9].

To check whether the oxygen dissociated from water vapour significantly affects the steel oxidation, Chandra-ambhorn et al. [4] oxidised a low carbon steel at 900 ºC in Ar-20% H_2O. As can be seen in Fig. 5.1, the equilibrium oxygen partial pressure is 8.45×10^{-7} bar in that atmosphere at 900 ºC. In their experiment, this gas mixture was flowed with the rate of 6 L h^{-1} to oxidise the steel in a thermobalance where the mass change was recorded every 5.3 s. The calculation showed that, within 5.3 s, the oxygen gas dissociated from water vapour is supplied to the reactor only with the amount of 0.0024 µg. However, H_2O in this atmosphere has the partial pressure of 0.2 bar. With the same gas flow rate, H_2O supplies oxygen associated with its molecule to the reactor with the amount of 290 µg in 5.3 s. The mass gain measured by thermobalance in each 5.3 s was found to be in the range of 1.4–27.0 µg [4]. These results indicate that water vapour plays a dominant role to provide oxygen for oxidation much more than the one from oxygen gas which is dissociated from water vapour.

When water vapour takes part in oxidation process, water is consumed and hydrogen is produced. These phenomena could change the ratio of water vapour to hydrogen ($p_{\mathrm{H_2O}} / p_{\mathrm{H_2}}$) in the atmosphere, and therefore possibly affect stability of the oxide formation. For the oxidation of metal M in H_2O giving M_aO_b, the global oxidation reaction can be written as follows:

$$aM + bH_2O \leftrightarrow M_aO_b + bH_2 \tag{5.3}$$

Let $dn_{H_2O,in}$ is the differential of the number of mole of water vapour that enters the reactor, $dn_{H_2O,consumed}$ is the differential of the number of mole of water vapour consumed by oxidation and $dn_{H_2,released}$ is the differential of the number of mole of hydrogen molecule produced as a result of the oxidation. If it is assumed that all hydrogen produced by Reaction 5.3 is released to the atmosphere, the p_{H_2O}/p_{H_2} at the time *t*, denoted as $(p_{H_2O}/p_{H_2})_t$, can be expressed as follows:

$$\left(\frac{p_{H_2O}}{p_{H_2}}\right)_t = \frac{dn_{H_2O,in} - dn_{H_2O,consumed}}{dn_{H_2,released}} \tag{5.4}$$

We can find out $dn_{H_2O,in}$ from the experimental parameters using the following relation:

$$dn_{H_2O,in} = \dot{n}_{H_2O,in}dt = \frac{p_{H_2O,in}\dot{V}}{RT}dt \tag{5.5}$$

where $p_{H_2O,in}$ is the partial pressure of water vapour entering the reactor, $\dot{V}$ is the gas flow rate, R is the ideal gas constant, T is the absolute temperature and dt is the differential of time. From Reaction 5.3, we see that the number of mole of H_2O consumed equals the number of mole of O used to form the oxide which is the one obtained from the experiment, thus giving

$$dn_{H_2O,consumed} = dn_{measured} \tag{5.6}$$

where $dn_{measured}$ is the differential of the number of mole measured from the thermogravimetric experiment. From Reaction 5.3, we can also see that the number of mole of H_2O consumed equals the number of mole of H_2 gas produced by the oxidation reaction. If it is assumed that all H_2 molecules produced from Reaction 5.3 release to the atmosphere, we can write that

$$dn_{H_2,released} = dn_{H_2O,consumed} \tag{5.7}$$

Substituting Eqs. 5.5–5.7 into Eq. 5.4 gives

$$\left(\frac{p_{H_2O}}{p_{H_2}}\right)_t = \frac{\dot{n}_{H_2O,in}dt}{dn_{measured}} - 1 \tag{5.8}$$

This equation shows that $dn_{measured}$, which depends on the oxidation kinetic behaviour of the metal influences $(p_{H_2O}/p_{H_2})_t$.

In the case of linear oxidation kinetics, the relation between mass gain $(\Delta m/A)$ and time (t) is expressed as

$$\left(\frac{\Delta m}{A}\right) = k_l t \tag{5.9}$$

where Δm is the difference between the mass measured at the time t and the mass before oxidation, A is the area of the metal and k_l is the linear rate constant. We can further derive that

$$\mathrm{d}n_{\mathrm{measured}} = \frac{Ak_l}{M_O}\mathrm{d}t \tag{5.10}$$

where M_O is the atomic mass of oxygen. Inserting Eq. 5.10 into Eq. 5.8 gives

$$\left(\frac{p_{H_2O}}{p_{H_2}}\right)_t = \frac{M_O\dot{n}_{H_2O,in}}{Ak_l} - 1 \tag{5.11}$$

From this equation, we can see that at a fixed flow rate and k_l, the $(p_{H_2O}/p_{H_2})_t$ gas ratio does not change with time. Furthermore, higher is the k_l, lower is the $(p_{H_2O}/p_{H_2})_t$.

In the case of parabolic oxidation, the relation between mass gain and time can be described as

$$\left(\frac{\Delta m}{A}\right)^2 = k_p t + \mathrm{C} \tag{5.12}$$

where k_p is the parabolic rate constant and C is a constant which could be obtained when fitting the experimental results. From this relation, it can be obtained that

$$\mathrm{d}n_{\mathrm{measured}} = \frac{k_p A\mathrm{d}t}{2M_O\sqrt{k_p t + \mathrm{C}}} \tag{5.13}$$

Inserting Eq. 5.13 into Eq. 5.8 gives

$$\left(\frac{p_{H_2O}}{p_{H_2}}\right)_t = \frac{2M_O\dot{n}_{H_2O,in}\sqrt{k_p t + \mathrm{C}}}{Ak_p} - 1 \tag{5.14}$$

From this equation, we can see that at the fixed gas flow rate, the $(p_{H_2O}/p_{H_2})_t$ increases parabolically with time.

Fig. 5.2 demonstrates the variation of $(p_{H_2O}/p_{H_2})_t$ as a function of time for steels oxidised at 900 ºC in Ar-20% H_2O [4]. In this case, the oxidation kinetics was found to be linear in the early stage, thus giving a constant $(p_{H_2O}/p_{H_2})_t$ as a function of time. After a linear oxidation stage, the kinetics turns into parabolic, thus giving an increased value of $(p_{H_2O}/p_{H_2})_t$ as function of time in accordance with the relation in Eq. 5.14. For $(p_{H_2O}/p_{H_2})_t$ in the range of 10^1 to $10^{2.5}$ (10–320), magnetite is a stable oxide phase. According to thermodynamic data from Ref. [9], this oxide phase is stable for p_{H_2O}/p_{H_2} in the range of 5.5–22422. However, haematite was found in experiment even though it is thermodynamically stable at the p_{H_2O}/p_{H_2} higher than 22422 [4]. It is possible that hydrogen produced by Reaction 5.3 is not totally released to the atmosphere. This thus causes, as described in Eq. 5.4, an increase of the $(p_{H_2O}/p_{H_2})_t$ up to a value corresponding to the stability domain of haematite. Furthermore, it should be noted that the variation of p_{H_2O}/p_{H_2} as analysed in

this section can be applied only if the gas pressure at the metal surface equals the bulk gas pressure value [10].

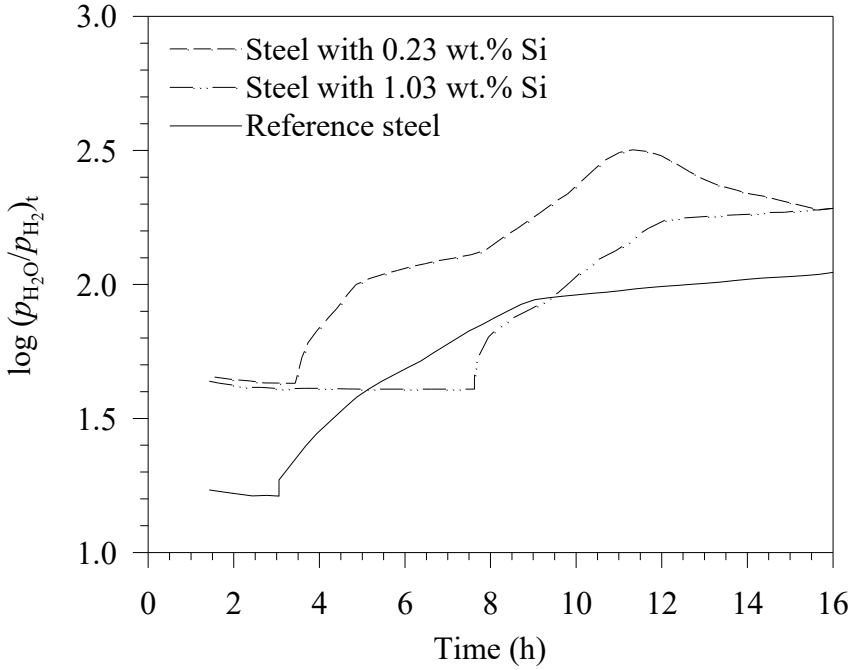

Fig. 5.2. Variation of $(p_{H_2O} / p_{H_2})_t$ as a function of time in the oxidation of steels at 900 ºC in Ar-20% H_2O. Redrawn from S. Chandra-ambhorn et al., Corros. Sci. 87 (2014) 101–110 [4].

5.2 Water Vapour Effect at the Solid/Gas Interface

5.2.1 Chromium Species Volatilisation

When water vapour from the bulk gas arrives at the metal surface it can oxidise the metal and also volatilise the oxide formed. Chromium species volatilisation, so-called chromium species evaporation or vaporisation, from chromia grown on chromium alloys in oxidising conditions at elevated temperatures has been observed by many researchers since 1960s. When chromium alloy was exposed to oxidising atmosphere at high temperatures, the CrO_3 crystal has sometimes been found to deposit at cooler parts of equipment due to the reduction of CrO_3 back to Cr_2O_3 [11, 12]. The research group of Caplan and Cohen [11] was one of the early groups who studied the chromium volatilisation by observing the weight loss of Cr_2O_3 pellets exposed to various dry and humidified atmospheres at 1000–1200 ºC for 5 to 100 h. In their experiment, the gas flow rate of gas was varied from 10 to 200 mL min^{-1} at room temperature, corresponding to a linear velocity in the range of 0.025–0.5 cm s^{-1}. They found for both dry and humidified oxygen that the rate of weight loss of Cr_2O_3 increased with increasing temperatures while no weight change occurred under dry and humidified argon atmospheres. They also found that the rate of weight loss of Cr_2O_3 exposed to humidified oxygen was about two times higher than in dry oxygen.

Tedmon [13] derived the model equation to describe the oxidation behaviour of chromium and iron-chromium alloys based on the assumption that not only chromium oxidation into Cr_2O_3 occurred when exposing to oxidising atmospheres at high temperatures but also the volatilisation of Cr_2O_3 formed into volatile species. By considering the two phenomena simultaneously, Tedmon found that a transition from a parabolic oxidation kinetics into linear one can be observed. This model is in good agreement with the experimental data.

Stearns et al. [14] measured the volatilisation rates of Cr_2O_3 at low pressure (1.51×10^{-4} atm) in gas steam with different partial pressures of oxygen over the temperature range of 1000–1300 ºC. Taking into account both diffusion and reaction effects, the reaction-controlled rates of chromium species volatilisation were calculated. They observed that the Cr_2O_3 volatilisation rate decreased

with decreasing oxygen partial pressure. Furthermore, they found a volatilisation rate dependence to the oxygen partial pressure to the power 0.75. For temperature dependence study, the Arrhenius relation between the Cr_2O_3 volatilisation rate versus reciprocal temperature gave the experimental activation energy of 251 ± 21 kJ mol^{-1}.

Fryburg et al. [15] investigated the formation of volatile species vaporised from various types of metals and alloys including chromium at 1050 ºC in oxidising atmospheres containing water vapour. They found that besides the volatile species of CrO_3, under the oxidising atmosphere containing water vapours, $CrO_2(OH)_2$ was also formed resulting in increasing the rate of chromium species evaporation.

Asteman et al. [16, 17] investigated chromium volatilisation from 304L stainless steel exposed to dry O_2 and O_2 containing 10% water vapour at 873 ºC from 1 to 672 h. The weight gain of the sample exposed to dry O_2 increased with increasing exposure time. They also observed that the presence of water vapour in O_2 did not significantly affect the weight gain for samples exposed for less than 168 h. However, for longer exposure time the weight gain of the samples exposed to wet O_2 was considerably lower than that exposed to dry O_2. They explained that after prolonged exposure to humidified oxygen, chromium species volatilisation and chromium-manganese spinel formation led to the decrease in the rate of weight gain. Chromium volatile species was suggested to be $CrO_2(OH)_2$.

Asteman et al. [18, 19] also investigated the effect of chromium species volatilisation on the oxidation behaviour of 304L and 310 steels in water vapour and oxygen mixtures at 500–800 ºC. In their experiment, the gas flow rate was varied. The results revealed that the oxidation strongly depended on the gas flow rate. In the oxidation of AISI 310 at 600 ºC in humidified oxygen using the gas flow rate in the range of 0.3–10 cm s^{-1}, they found that at relatively low gas flow rate the protective α-$(Cr,Fe)_2O_3$ oxide was formed with the outer part depleted in chromium. At high flow rates beyond the critical value the protective oxide could be failed [19]. In that case, the α-$Fe_2O_3/(Cr,Fe)_2O_3$ with the thickness higher than 5 μm was found at the heart of the alloy grain while the α-$(Cr,Fe)_2O_3$ close to the steel grain boundaries remained partially protective. They further suggested that durability of stainless steel in humidified oxygen is connected to its ability to compensate chromium loss by sublimation.

Yamauchi et al. [20] also investigated the effect of water vapour on the volatilisation of chromia. Their results were in good agreement with Asteman et al. [16, 17]. Furthermore, they compared the volatilisation behaviour of chromia under N_2-O_2-H_2O atmosphere with those under N_2-O_2 and N_2-H_2O atmospheres within the temperature range of 1173–1473 K. In their work, samples were prepared by hot-pressing chromia powder in a graphite die using sintering temperature of 1673 K. Before the test, all samples were polished with a fine diamond abrasive and then ultrasonically cleaned in ethanol. Mass loss of each sample was measured for various exposure times. It was observed that the mass losses in N_2-O_2 and N_2-H_2O atmospheres were almost identical and very low in comparison with that in N_2-O_2-H_2O atmosphere. From this observation, they suggested that the chromium species volatilisation based on the reaction that both oxygen and water vapour were involved. Considering the effect of oxygen partial pressure on the mass loss, they found that the rate of mass loss increased with increasing oxygen partial pressure.

Gindorf et al. [21] developed the transpiration apparatus used to measure the amount of vaporised chromium species. They measured the amount of chromium species evaporated from Cr_2O_3 powder at 1223 K at different flow rates of humid air. They observed that a chromium sublimation rate increases with increasing flow rate. However, the chromium volatilisation rate remains unchanged for flow rate higher than 400 mL min^{-1}. Gindorf et al. also performed the thermodynamic computation using databases of IVTANTHERMO and Ebbinghaus and found that most abundant volatilisation reactions should be as follows:

$$Cr_2O_{3(s)} + \frac{3}{2}O_{2(g)} \rightarrow 2CrO_{3(g)} \quad (5.15)$$

$$Cr_2O_{3(s)} + \frac{3}{2}O_{2(g)} + 2H_2O_{(g)} \rightarrow 2CrO_2(OH)_{2(g)} \quad (5.16)$$

$$Cr_2O_{3(s)} + O_{2(g)} + H_2O_{(g)} \rightarrow 2CrO_2(OH)_{(g)} \quad (5.17)$$

Furthermore, they compared their experimental results with the computational one and found that, at low partial pressure of water vapour, the evaporated chromium species is in the form of CrO_3 while, at high partial pressure of water vapour, $CrO_2(OH)_2$ should be major chromium volatile species.

Opila et al. [22] studied the effect of oxygen and water vapour partial pressure on the amount of produced chromium volatile species. They found that partial pressure of the chromium volatile species depended on the partial pressure of water vapour to the power 0.96 and partial pressure of O_2 to the power 0.77. These values corresponded to the power law exponents of the rate law of Reaction 5.16. Kurokawa et al. [23] also investigated the effect of gas flow rate on the amount of chromium species volatilisation from chromium oxide pellets using experimental setup inspired by the transpiration apparatus of Gindorf's research group. Their results are in agreement with the ones by Gindorf et al. [21].

Stanislowski et al. [24] studied chromium species volatilisation on the surface of chromia-forming Ducrolloy exposed to humidified air at 800 ºC by varying the flow rate from laminar to turbulent regime. The evolution of chromium volatilisation flux according gas flow rate can be divided into three zones called "equilibrium volatilisation", "non-equilibrium volatilisation" and "volatilisation limit". For the "equilibrium volatilisation" related to the lower flow rate part of laminar flow region, the reactions are at equilibrium. The rates of forward and backward reactions are equivalent. Hence, chromium species volatilisation rate should be equal to the one calculated by thermodynamics, and thus increases with increasing the gas flow rate. In the "non-equilibrium volatilisation" zone that covers higher flow rate part of laminar flow region and the beginning part of turbulent zone, a thin film of gas called "boundary layer" forms on the surface. A concentration gradient happens due to the diffusion limit of chemical species with boundary layer. In laminar regime, both inside and outside boundary layers have laminar flow pattern. The faster the gas flows, the thinner the boundary layer is formed resulting in less concentration gradient. At the beginning when the laminar flow changes into the turbulent flow due to the increase of fluid flow rate, the flow pattern at the top part of boundary layer becomes turbulent while the bottom part of boundary layer which is close to the surface still maintains laminar flow pattern. In the turbulent zone of boundary layer, a turbulent stream causes the fluid to well mix. Therefore, a concentration gradient in the turbulent zone becomes less as the degree of turbulent increases. This may be the reason why chromium species volatilisation rate increases with increasing rate at first and then the increasing rate becomes slower as the flow is more turbulent. For the last zone, volatilisation limit zone, the flow is fully turbulent and, instead of diffusion limit, chromium volatilisation is limited by kinetics.

In our research group, Wongpromrat et al. [6] developed the experimental set-up as described in Section 3.3 in Chapter 3 to measure the chromium species volatilisation from AISI 430 stainless steel subjected to O_2-5% H_2O at 800 ºC. It was found that in the linear gas velocity range of 0.8–1.95 cm s^{-1}, the chromium species volatilisation rate increases with the increased velocity as shown in Fig. 5.3. This indicates that the mass transfer rate of the chromium volatile specie is slower than the surface reaction rate. Thus the mass transfer of the volatile specie across the oxide/gas interface is a rate-determining step.

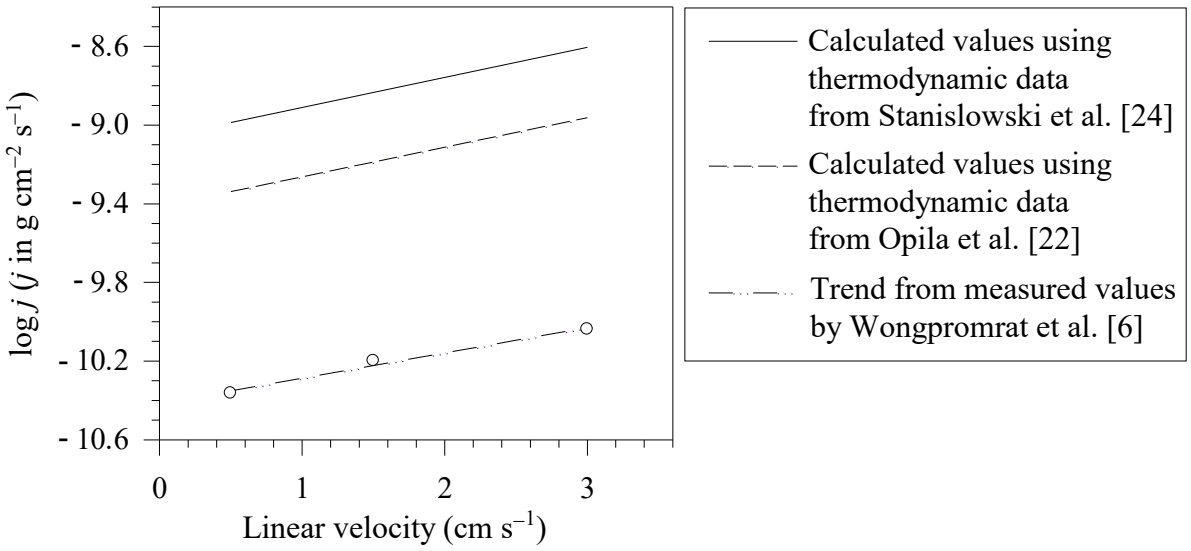

Fig. 5.3. Mass flux of the Cr volatile species (j) measured from AISI 430 oxidised at 800 ºC in O_2-5% H_2O for 24 h [6] compared with the mass fluxes calculated using thermodynamic data from Opila et al. [22] and Stanislowski et al. [24]. Redrawn and adapted from W. Wongpromrat et al., Oxid. Met. 79 (2013) 529–540.

To compare the results with the theoretical value, mass flux of the chromium volatile species (j) is calculated using the following equation [6, 25]:

$$j = \frac{k_{\mathrm{m}}}{\mathrm{R}T}(p_{\mathrm{surface}} - p_{\mathrm{bulk}}) \tag{5.18}$$

Here, k_{m} is the mass transfer coefficient of the chromium volatile species, R is the ideal gas constant, T is the absolute temperature. p_{surface} and p_{bulk} are the partial pressures of the volatile species at the solid surface and in the bulk gas respectively.

In the following calculation of the mass flux, it is assumed that p_{surface} is significantly higher than p_{bulk} and thus the p_{bulk} term is neglected. The values of p_{surface} can be obtained by using thermodynamic data reported in literature. As for k_{m}, its value can be obtained from Eq. 5.19 [6, 25] where v is the kinematic viscosity, v_{l} is the linear velocity of the gas and l is the sample length. D_{AB} is the binary gas (O_2-$CrO_2(OH)_2$) diffusion coefficient which can be calculated using the Chapman-Enskog kinetic theory [26]. The calculation shows that the values of k_{m} are 0.5–1.5 cm s^{-1} for the linear velocity of the gas in the range of 0.85–1.95 cm s^{-1}.

$$k_{\mathrm{m}} = 0.664\left(\frac{D_{\mathrm{AB}}}{v}\right)^{\frac{1}{6}}\left(\frac{\mathrm{v_l}}{l}\right)^{\frac{1}{2}} \tag{5.19}$$

By determining the values of k_{m}, p_{surface} and p_{bulk} previously discussed as well as T, the mass flux of the volatile specie according to Eq. 5.18 can be calculated and plotted in Fig. 5.3. In that figure, there are also two calculated lines which were obtained by using different thermodynamic data i.e. from Opila et al. [22] and Stanislowski et al. [24] in order to find out the value of p_{surface}. It can be seen that our measured mass fluxes are lower than the calculated ones. The measured mass fluxes were obtained from the chromium volatile species in the bulk gas which was dissolved in water and washing solution as described in Section 3.3 in Chapter 3, while the calculated mass flux is the flux that transfers from the solid surface to the bulk gas. The volatilisation in this case is controlled by

mass transfer of the volatile species, therefore the mass flux of the volatile species in the bulk gas which was the measured value was lower than the mass flux passing through the oxide/gas interface which is calculated using Eq. 5.18.

Wongpromrat et al. [7] also investigated the effect of gas velocity on the chromium species volatilisation rate of the AISI 441 stainless steel up to the linear gas velocity of 10 cm s^{-1}. The result is shown in Fig. 5.4. As seen from the figure, the pattern of the graph is similar to the results of Gindorf et al. [21] and Kurokawa et al. [23] i.e. at the low linear velocity range of 1–4 cm s^{-1}, volatilisation rate increases with increasing gas velocity. Meanwhile, at the gas velocity more than 4 cm s^{-1}, volatilisation rate seems unchanged. They explained that, at low gas velocity, volatilisation rate is limited by the diffusion rate of chromium volatile species through the boundary layer, while at high gas velocity, diffusion rate becomes faster resulting in constant volatilisation rate as it is limited by surface reaction. Comparing with the result of Stanislowski et al. [24], it is possible that Gindorf et al. [21] and Kurokawa et al. [23] and Wongpromrat et al. [7] performed the experiments at low velocity which might lie on "laminar region" discussed in Stanislowski et al. [24] as they performed the experiments with low gas velocities.

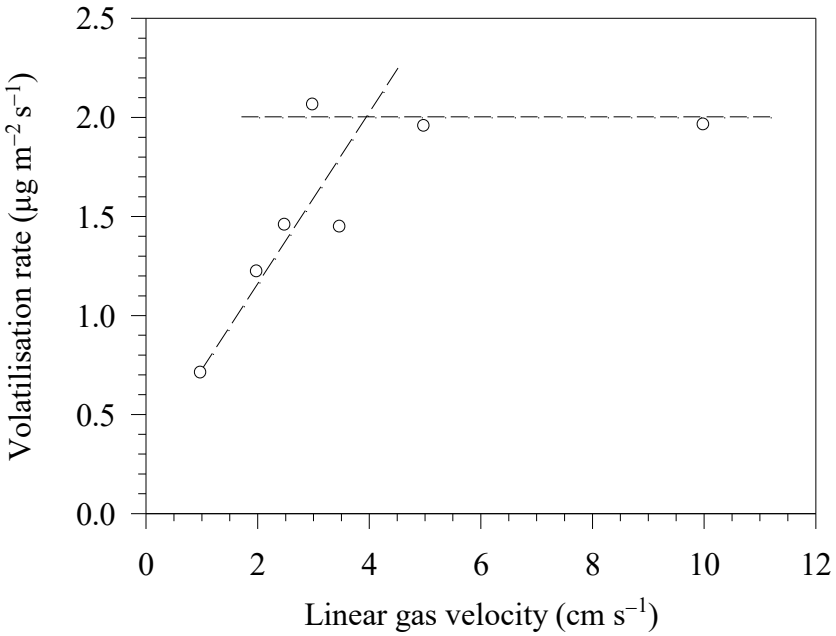

Fig. 5.4. Chromium species volatilisation rate of the AISI 441 oxidised at 800 ºC in O_2-5% H_2O for 96 h as a function of linear gas velocity. Redrawn from W. Wongpromrat et al., Corros. Sci. 106 (2016) 172–178 [7].

Expecting to reduce the chromium species volatilisation rate of AISI 441, Wongpromrat et al. coated their specimens with Mn–Co spinel and found that unlike the case of AISI 430, Mn–Co spinel coating could not suppress the chromium volatilisation [6]. Therefore, under the supervision of Professor Alain Galerie and the collaboration between KMITL, KMUTNB (Bangkok, Thailand) and SIMaP (Grenoble, France), instead of using conventional way like coating the steel surface with ceramics, Wongpromrat et al. [7] applied the pre-oxidation method to form thin pre-oxidation film on AISI 441. As seen in Figs. 5.5 and 5.6, superior suppression of chromium species volatilisation is obtained when flowing 5% H_2O in O_2 at low rates (0–4 cm s^{-1}) for 96 h through the pre-oxidised specimens in argon at 250 ºC and in CO_2/CO at 250 and 850 ºC. This means that the pre-oxidation could be a promising method to inhibit chromium species volatilisation from AISI 441 which will probably be able to use as interconnector of solid oxide electrochemical devices. The possible mechanism for this suppression is described in Section 6.4 in Chapter 6 concerning the chromium volatilisation of stainless steel SOFC interconnect.

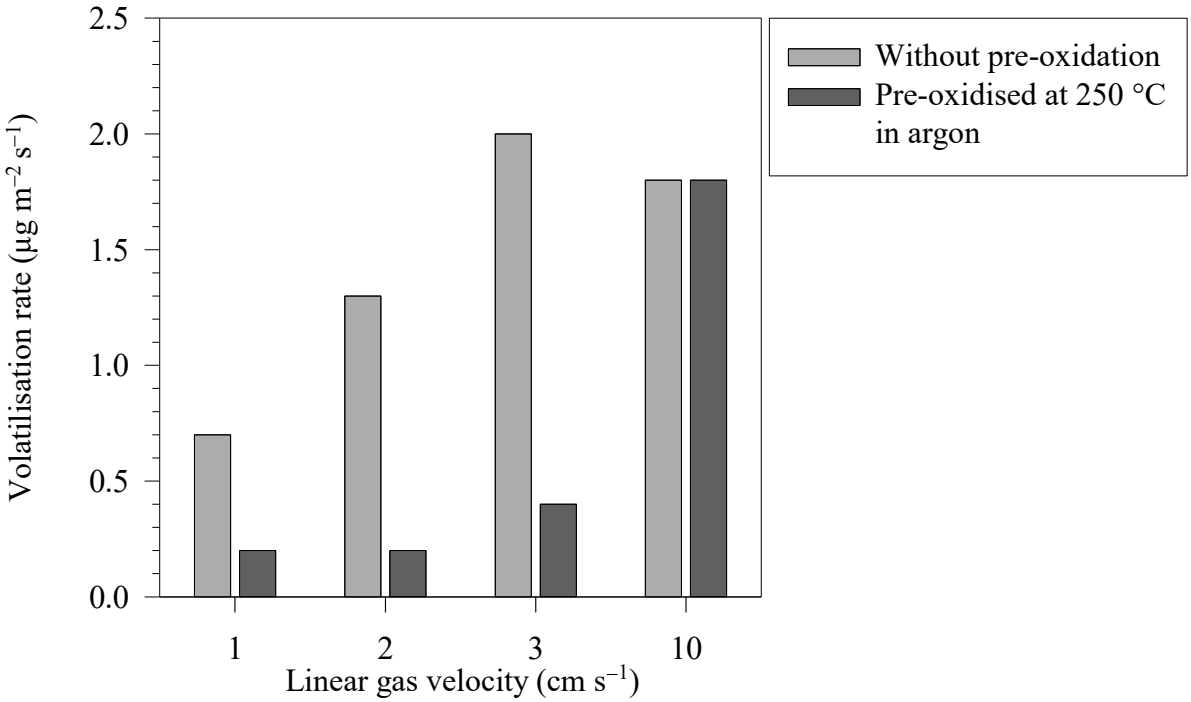

Fig. 5.5. Chromium species volatilisation rate of the AISI 441 without and with pre-oxidation in argon at 250 ºC after exposure to O_2-5% H_2O at 800 ºC for 96 h. Redrawn from W. Wongpromrat et al., Corros. Sci. 106 (2016) 172–178 [7].

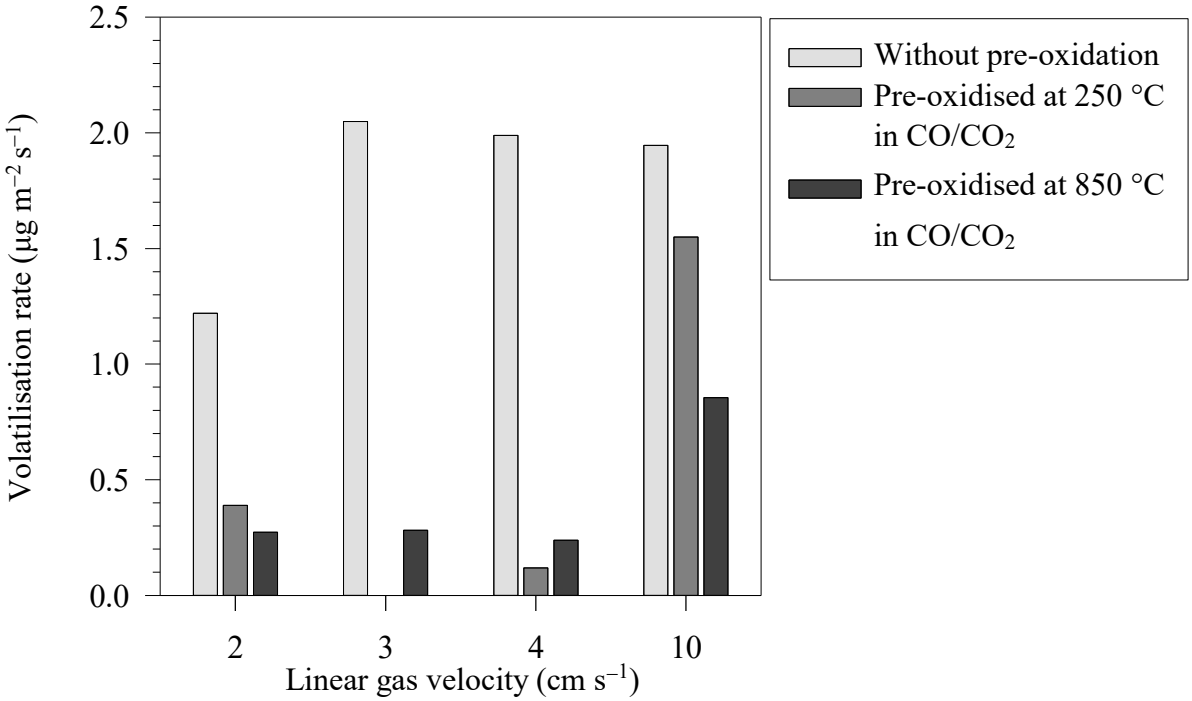

Fig. 5.6. Chromium species volatilisation rate of AISI 441 without and with pre-oxidation in CO/CO_2 at 250 and 850 ºC after exposure to O_2-5% H_2O at 800 ºC for 96 h. Redrawn from W. Wongpromrat et al., Corros. Sci. 106 (2016) 172–178 [7].

5.2.2 Oxidation Controlled by Surface Reaction

Water vapour could not only volatilise the oxide on the surface but also oxidise the metal. When water vapour does not impact the diffusion process or modify the microstructure of the oxide, the surface reaction can be a rate determining step for the oxidation process [27]. In pure water vapour, Galerie et al. [8] and Young [27] suggested that water vapour can be dissociated giving OH

adsorbed on the site s ($OH-s$) and H_2 at the solid/gas interface according to Reaction 5.20. The adsorbed OH could further dissociate giving the adsorbed O and H_2 according to Reaction 5.21. They suggested that the energy needed to break the first OH bond is significantly lower than the one needed to break the second OH bond. As a result, the covering of hydroxide on the surface is more probable even at room temperature, while the covering of oxygen on the surface is less likely [8]. The oxygen species need the surface that can tightly fix the OH particle by its oxygen electron pair so that, by the great induced polarisation, the second OH bond can be broken; and in such case the surface is acidic [8]. Galerie et al. [8] plotted the evolution of a linear rate constant of metals oxidised in water vapour with the cation hydration enthalpies, giving the linear relationship between these two variables as shown in Fig. 5.7. It is noted that the oxidation rate of chromium and niobium are in fact parabolic, but a linear mean rate is assumed in the first 1 h [8]. From this figure, they proposed to use the cation hydration enthalpy to assess the acidity of the oxide in the manner that more negative value of the cation hydration enthalpy indicates more acidity of the oxide, and as a consequence the faster oxidation rate.

$$H_2O_{(g)} + s \rightarrow OH - s + \frac{1}{2}H_{2(g)} \tag{5.20}$$

$$OH - s \rightarrow O - s + \frac{1}{2}H_{2(g)} \tag{5.21}$$

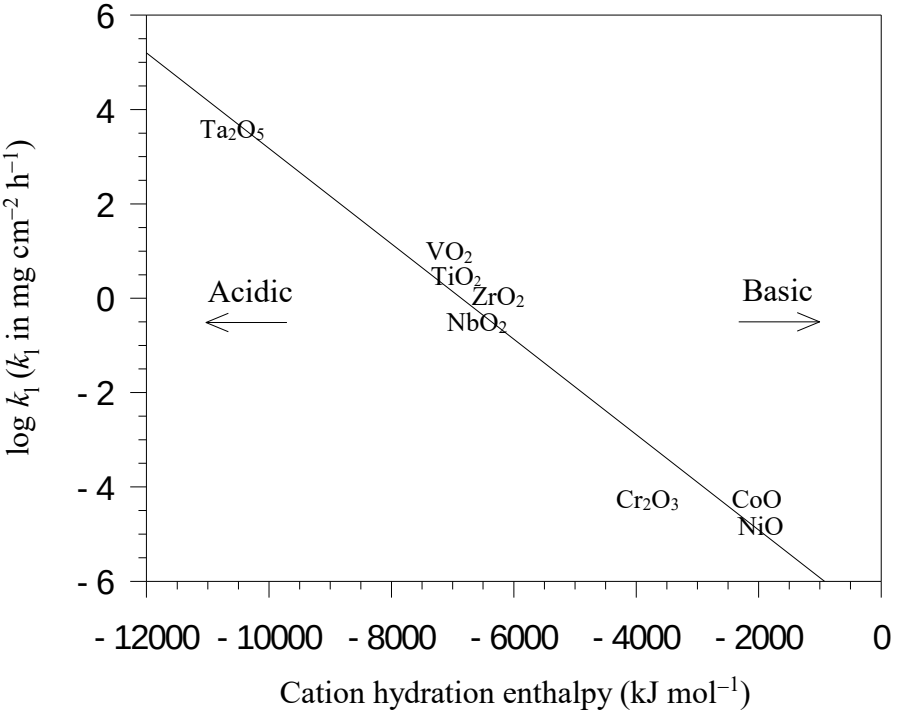

Fig. 5.7. Relation between the linear rate constant for the oxidation of metals in water vapour at 800 ºC and the cation hydration enthalpies. Redrawn from A. Galerie et al., Mater. Sci. Forum 369–372 (2001) 231–238 [8].

However, the prediction of the oxidation rate using the hydration enthalpy is limited by many reasons such as the oxides formed in oxygen and in water vapour must be in the same form so that the comparison is relevant [8]. The prediction cannot be used for the case of vanadium and niobium since these metals form V_2O_5 and Nb_2O_5 in oxygen, while they form VO_2 and NbO_2 in water vapour [8]. In the case of chromia, the diffusion in this oxide is relatively slow and remains a rate

determining step for the oxidation in water vapour [27], even though in some other atmospheres like carbon-containing ones, the surface reaction can be a rate determining step for stainless steel oxidation [28–30] as described in Section 6.3.2.2 in Chapter 6. Furthermore, water vapour significantly changes the defect structure and therefore the diffusion process, as well as the microstructure of Cr_2O_3. These changes influence the oxidation mechanism as will be explained in the next section.

5.3 Water Vapour Effect on the Diffusion-Controlled Oxidation through Chromia

5.3.1 Diffusion-Controlled Oxidation Phenomena

Figs. 5.8–5.10 exemplifies the effect of water vapour on the oxidation of iron, chromium and iron-chromium alloys at high temperatures. Fig. 5.8 shows the mass gain of iron when it was oxidised in oxygen without and with water vapour [31]. It can be seen that, at relatively low temperature of 700 ºC, the oxidation rates of iron in both atmospheres are nearly identical. However, at the higher temperatures of 800 and 900 ºC, water vapour in the atmosphere accelerates the iron oxidation rate.

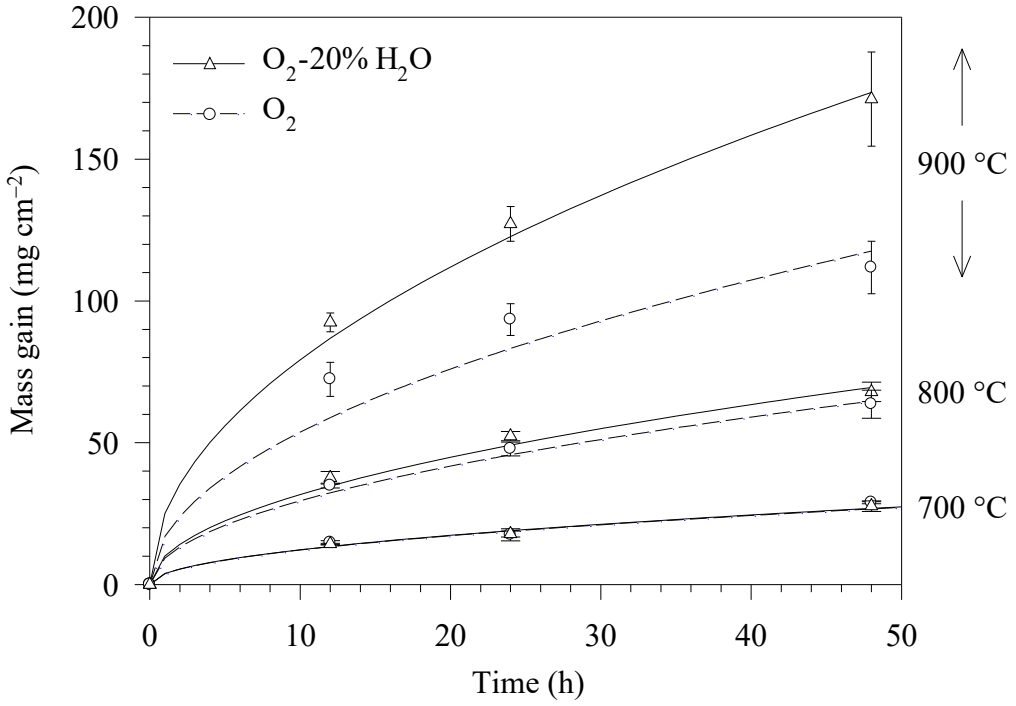

Fig. 5.8. Mass gains of iron oxidised in dry and humidified oxygen at 700, 800 and 900 °C. Redrawn and adapted from S. Chandra-ambhorn et al., Corros. Sci. 148 (2019) 355–365 [31].

For the chromia thermally grown on chromium, Hänsel et al. [32] conducted the oxidation test at 1000 ºC in argon containing water vapour, oxygen and hydrogen. The oxidation kinetics was found to be parabolic. For the results at relatively high oxygen partial pressure i.e. 0.04 bar, the parabolic rate constant is independent on the water vapour content as shown in Fig. 5.9. However, at the relatively low oxygen partial pressure in the range of 10^{-15} to 10^{-14} bar, three important results were observed. First, the rate constant increases with the increased water vapour content at constant oxygen partial pressure as shown in Fig. 5.10(a). Second, the rate constant increases with the increased water vapour at constant hydrogen partial pressure as in Fig. 5.10(b). Third, the rate constant increases with the increased hydrogen partial pressure at constant oxygen partial pressure as in Fig. 5.10(c). It is noted that the oxygen partial pressure in Figs. 5.9 and 5.10 were calculated using thermodynamic data from Ref. [9].

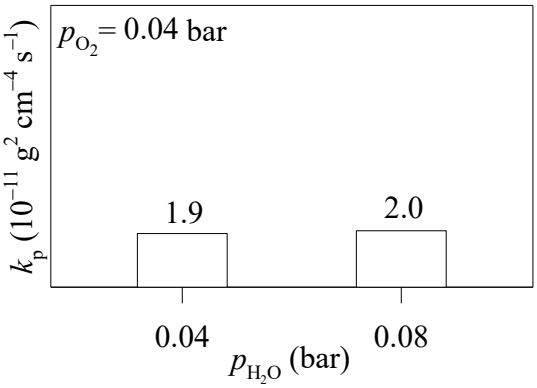

Fig. 5.9. Parabolic rate constant as a function of the partial pressure of water vapour at constant oxygen partial pressure for the chromium oxidation at 1000 ºC in the relatively high oxygen partial pressure [32].

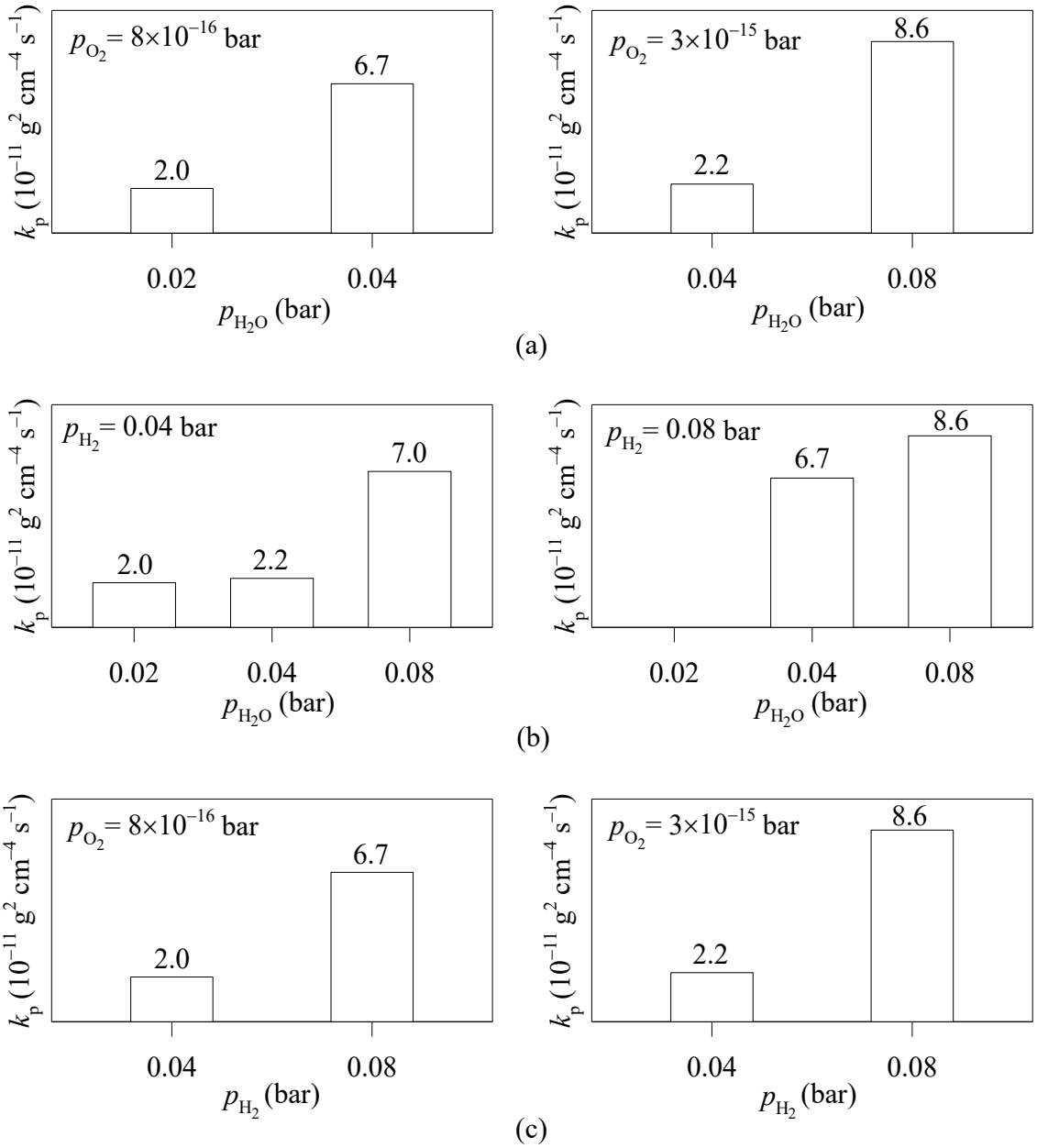

Fig. 5.10. Parabolic rate constant as a function of (a) the partial pressure of water vapour at constant oxygen partial pressure (b) the partial pressure of water vapour content at constant hydrogen partial pressure, and (c) the hydrogen partial pressure at constant oxygen partial pressure for the chromium oxidation at 1000 ºC in the relatively low oxygen partial pressure range [32].

Fig. 5.11 shows the oxidation behaviour of Fe–15.7Cr–8.5Mn stainless steel in dry and humidified oxygen at 700 ºC [33]. The kinetics is also found to be parabolic with the enhanced rate when water vapour presents in the atmosphere. This result was also observed such as in the case of Fe–17Cr–1Mn stainless steel [34]. According to Figs. 5.8–5.11, the oxidation rate is parabolic which indicates that the oxidation is controlled by the diffusion through the oxide.

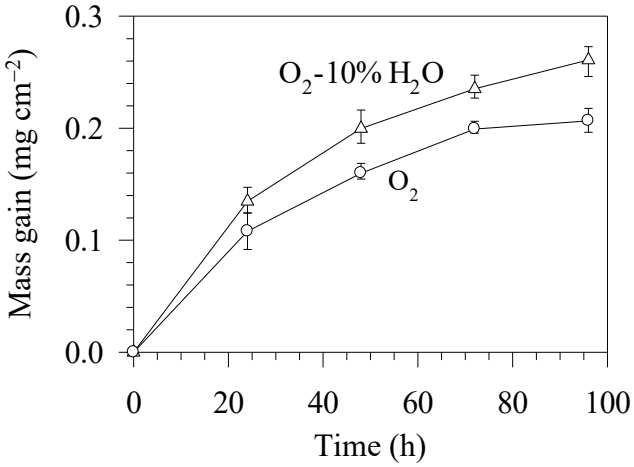

Fig. 5.11. Mass gains of Fe–15.7Cr–8.5Mn stainless steel oxidised in dry and humidified oxygen at 700 ºC. Redrawn and adapted from S. Chandra-ambhorn, Corros. Sci. 148 (2019) 39–47 [33].

To understand the role of water vapour on defect structure and therefore the oxidation mechanism, we start from the simple case of an oxide in the form of M_2O_3 where metal vacancy is a dominant defect at the outer part and oxygen vacancy is a major defect in the inner part of the oxide. This defect structure is in agreement with Cr_2O_3 formed in oxygen as described in Section 4.1.2 in Chapter 4. The relevant defect formation reactions are shown in Reactions 5.22 and 5.23. These two reactions give the Schottky defect reaction as shown in Reaction 5.24. The electronic defect reaction also exists in the oxide as shown in Reaction 5.25.

$$\frac{3}{2}O_2 \leftrightarrow 3O_O + 2V_M''' + 6h^\bullet \tag{5.22}$$

$$\frac{3}{2}O_2 + 3V_O^{\bullet\bullet} + 6e' \leftrightarrow 3O_O \tag{5.23}$$

$$\text{nil} \leftrightarrow 2V_M''' + 3V_O^{\bullet\bullet} \tag{5.24}$$

$$\text{nil} \leftrightarrow e' + h^\bullet \tag{5.25}$$

When water vapour presents in the atmosphere, water vapour might be incorporated in the oxide in many forms, at least in the following three cases: (i) an incorporation of water vapour in the form of the hydrogen interstitial with positively unit effective charge ($H_i^\bullet$) [35, 36], (ii) a formation of $H_i^\bullet$ which is bounded with oxygen in the oxide giving the substitutional hydroxyl ion ($OH_O^\bullet$) together with the hydrogen interstitial with negatively unit effective charge (H_i') [32], and (iii) a formation of the hydroxyl ion which plays a major role on enhancing the oxygen inward diffusion [8, 37]. Each possibility will be discussed as follows.

5.3.2 Defect Structural Analysis when $H_i^\bullet$ Presents in M_2O_3

Norby [35] proposed the beautiful analysis leading to the construction of the Brouwer diagram for M_2O_3 oxidised in humidified oxygen which is a framework of this section. It was argued that

water vapour in the atmosphere could dissociate giving hydrogen interstitial and liberate oxygen according to Reaction 5.26 [35]. From this reaction and Reaction 5.1, we may consider that water vapour could dissociate giving hydrogen gas according to Reaction 5.1 and the hydrogen gas dissolves into the oxide in the hydrogen interstitial form according to Reaction 5.27 [35].

$$\frac{1}{2}H_2O \leftrightarrow H_i^{\bullet} + \frac{1}{4}O_2 + e' \tag{5.26}$$

$$\frac{1}{2}H_2 \leftrightarrow H_i^{\bullet} + e' \tag{5.27}$$

From Reactions 5.22 and 5.26, Reaction 5.28 showing the relation between metal vacancy and hydrogen interstitial can be obtained. Similarly, from Reactions 5.23 and 5.26, we can have Reaction 5.29 which shows the relation between oxygen vacancy and hydrogen interstitial.

$$3H_2O \leftrightarrow 3O_O + 2V_M''' + 6H_i^{\bullet} \tag{5.28}$$

$$3H_2O + 3V_O^{\bullet\bullet} \leftrightarrow 3O_O + 6H_i^{\bullet} \tag{5.29}$$

Equilibrium constants of some reactions used in the following analysis are given in Eqs. 5.30–5.35. $K_{5.22}$, $K_{5.23}$, $K_{5.26}$, $K_{5.28}$ are the equilibrium constants of Reactions 5.22, 5.23, 5.26 and 5.28, respectively. K_S is the equilibrium of the Schottky defect reaction according to Reaction 5.24, while K_e is the equilibrium constant of the electronic defect reaction according to Reaction 5.25.

$$K_{5.22} = \frac{[V_M''']^2[h^{\bullet}]^6}{p_{O_2}^{3/2}} \tag{5.30}$$

$$K_{5.23} = \frac{1}{[V_O^{\bullet\bullet}]^3[e']^6 p_{O_2}^{3/2}} \tag{5.31}$$

$$K_{5.26} = \frac{[H_i^{\bullet}][e']p_{O_2}^{1/4}}{p_{H_2O}^{1/2}} \tag{5.32}$$

$$K_{5.28} = \frac{[V_M''']^2[H_i^{\bullet}]^6}{p_{H_2O}^{3}} \tag{5.33}$$

$$K_S = [V_M''']^2[V_O^{\bullet\bullet}]^3 \tag{5.34}$$

$$K_e = [e'][h^{\bullet}] \tag{5.35}$$

Norby [35] assumed that at relatively lower partial pressure of water, hydrogen interstitial is a minor defect (case I). Reaction 5.29 shows that, in this condition, the oxygen vacancy becomes dominant. Its charge is compensated by electron as can be seen from Reaction 5.23. When the partial pressure of water vapour increases, Norby proposed that hydrogen interstitial became dominant and was compensated by electron (case II) and eventually by metal vacancy (case III) as can be seen from Reaction 5.28. From these assumptions, the dependencies of defect concentrations with the gas partial pressures can be derived as follows.

For the case I corresponding to the condition that hydrogen interstitial is a minor defect, the electroneutrality condition is

$$[e'] = 2[V_O^{\bullet\bullet}] \tag{5.36}$$

From Eqs. 5.31 and 5.36, it can be obtained that

$$[V_O^{\bullet\bullet}] = \frac{1}{2^{2/3} K_{5.23}^{1/9}} \cdot \frac{1}{p_{O_2}^{1/6}} \tag{5.37}$$

From Eqs. 5.34 and 5.37, we obtain that

$$[V_M^{\prime\prime\prime}] = (2K_{5.23}^{1/6} K_S^{1/2}) \cdot p_{O_2}^{1/4} \tag{5.38}$$

From Eqs. 5.36 and 5.37, it can be obtained that

$$[e'] = \frac{2^{1/3}}{K_{5.23}^{1/9}} \cdot \frac{1}{p_{O_2}^{1/6}} \tag{5.39}$$

From Eqs. 5.35 and 5.39, it can be obtained that

$$[h^{\bullet}] = \frac{K_{5.23}^{1/9} K_e}{2^{1/3}} \cdot p_{O_2}^{1/6} \tag{5.40}$$

From Eqs. 5.32 and 5.39, we can obtain that

$$[H_i^{\bullet}] = \frac{K_{5.23}^{1/9} K_{5.26}}{2^{1/3}} \cdot \frac{p_{H_2O}^{1/2}}{p_{O_2}^{1/12}} \tag{5.41}$$

For the case II corresponding to the condition that hydrogen interstitial is the major defect compensated by electron, the electroneutrality condition is

$$[e'] = [H_i^{\bullet}] \tag{5.42}$$

From Eqs. 5.32 and 5.42, the following relation is obtained:

$$[e'] = [H_i^{\bullet}] = K_{5.26}^{1/2} \cdot \frac{p_{H_2O}^{1/4}}{p_{O_2}^{1/8}} \tag{5.43}$$

From Eqs. 5.35 and 5.43, it can be obtained that

$$[h^{\bullet}] = \frac{K_e}{K_{5.26}^{1/2}} \cdot \frac{p_{O_2}^{1/8}}{p_{H_2O}^{1/4}} \tag{5.44}$$

From Eqs. 5.31 and 5.43, we can obtain that

$$[V_O^{\bullet\bullet}] = \frac{1}{K_{5.23}^{1/3} K_{5.26}} \cdot \frac{1}{p_{H_2O}^{1/2} p_{O_2}^{1/4}} \tag{5.45}$$

From Eqs. 5.34 and 5.45, we obtain

$$[V_M^{\prime\prime\prime}] = (K_{5.23}^{1/2} K_{5.26}^{3/2} K_S^{1/2}) \cdot p_{H_2O}^{3/4} p_{O_2}^{3/8} \tag{5.46}$$

For the case III corresponding to the condition that hydrogen interstitial is the major defect compensated by metal vacancy, the electroneutrality condition is

$$3[V_M'''] = [H_i^\bullet] \tag{5.47}$$

From Eqs. 5.33 and 5.47, it can be obtained that

$$[V_M'''] = \frac{K_{5.28}^{1/8}}{3^{3/4}} \cdot p_{H_2O}^{3/8} \tag{5.48}$$

From Eqs. 5.47 and 5.48 we can obtain that

$$[H_i^\bullet] = (3^{1/4} K_{5.28}^{1/8}) \cdot p_{H_2O}^{3/8} \tag{5.49}$$

From Eqs. 5.34 and 5.48 we obtain

$$[V_O^{\bullet\bullet}] = \frac{3^{1/2} K_S^{1/3}}{K_{5.28}^{1/12}} \cdot \frac{1}{p_{H_2O}^{1/4}} \tag{5.50}$$

From Eqs. 5.32 and 5.49, it can be obtained that

$$[e'] = \frac{K_{5.26}}{3^{1/4} K_{5.28}^{1/8}} \frac{p_{H_2O}^{1/8}}{p_{O_2}^{1/4}} \tag{5.51}$$

From Eqs. 5.35 and 5.51, we can obtain

$$[h^\bullet] = \frac{3^{1/4} K_{5.28}^{1/8} K_e}{K_{5.26}} \cdot \frac{p_{O_2}^{1/4}}{p_{H_2O}^{1/8}} \tag{5.52}$$

From Eqs. 5.37–5.41, 5.43–5.46 and 5.48–5.52, the defect concentrations can also be plotted as a function of the oxygen partial pressure at a fixed water vapour pressure, giving the Brouwer diagram as shown in Fig. 5.12. This diagram is similar to the one presented by Norby [35] but with slight correction to make all lines follow Eqs. 5.36–5.52.

Based on this analysis, Chandra-ambhorn et al. [33] proposed the graphical representation of the role of water vapour on the defect concentrations and dominant regimes as illustrated in Fig. 5.13 [33]. When water vapour content in the atmosphere increases, the defect concentration lines shift from the solid to the dash ones. The shifts of these lines further change the dominant regime of each defect by shifting the vertical dotted lines which separate each dominant defect area.

$$[e'] = 2[V_O^{\bullet\bullet}] \qquad [e'] = [H_i^\bullet] \qquad 3[V_M'''] = [H_i^\bullet]$$

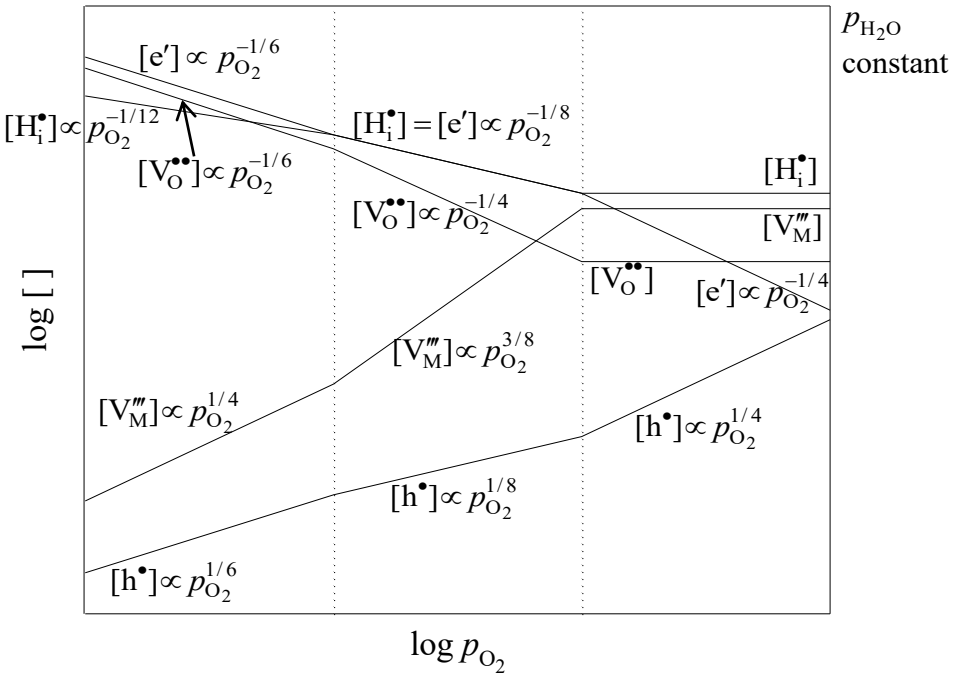

Fig. 5.12. Brouwer diagram for M_2O_3 in humidified oxygen based on Norby's work [35]. Redrawn from S. Chandra-ambhorn et al., Corros. Sci. 148 (2019) 39–47 [33].

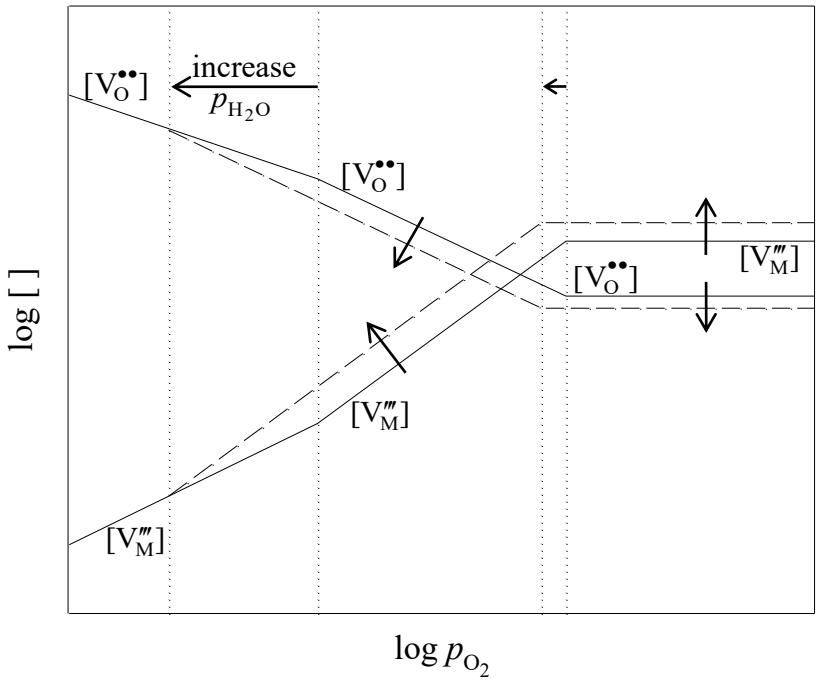

Fig. 5.13. The effect of water vapour on metal and oxygen vacancy concentrations in a Brouwer diagram. Redrawn from S. Chandra-ambhorn et al., Corros. Sci. 148 (2019) 39–47 [33].

It can be seen from Fig. 5.13 that in the relatively high water vapour content region (case III), when water vapour content increases the metal vacancy concentration increases and the dominant regime of this defect is expanded. If the metal vacancy is dominant for the oxide growth, the increase in its concentration enhances the oxidation rate of the metal.

5.3.3 Defect Structural Analysis when $OH_O^{\bullet}$ and $H_i^{\prime}$ Presents in M_2O_3

In this analysis, Hänsel et al. [32] proposed the defect situations in chromia, which are the framework of this section, to explain the results shown in Figs. 5.9 and 5.10. When $V_M^{\prime\prime\prime}$ is the dominant defect, the defect formation reaction is like Reaction 5.22. It is still considered that water vapour gives the hydrogen defect in the oxide. However, if hydrogen interstitial is bounded with the oxygen atom in the crystal, Reaction 5.27 could be re-written as Reaction 5.53 with the equilibrium constant shown in Eq. 5.54.

$$\frac{1}{2}H_2 + O_O + h^{\bullet} \leftrightarrow OH_O^{\bullet} \tag{5.53}$$

$$K_{5.53} = \frac{[OH_O^{\bullet}]}{[h^{\bullet}]p_{H_2}^{1/2}} \tag{5.54}$$

The charge balance condition in this case is written as

$$3[V_M^{\prime\prime\prime}] = [OH_O^{\bullet}] + [h^{\bullet}] \tag{5.55}$$

From Eqs. 5.30, 5.54 and 5.55, it can be obtained that

$$[V_M^{\prime\prime\prime}] = \frac{K_{5.22}^{1/8}}{3^{3/4}} \cdot p_{O_2}^{3/16} \cdot (1 + K_{5.53}p_{H_2}^{1/2})^{3/4} \tag{5.56}$$

From Eq. 5.56 and the equilibrium constant of water dissociation from Eq. 5.2, it can be obtained that

$$[V_M^{\prime\prime\prime}] = \frac{K_{5.22}^{1/8}K_w^{3/8}}{3^{3/4}} \cdot \frac{p_{H_2O}^{3/8}}{p_{H_2}^{3/8}} \cdot (1 + K_{5.53}p_{H_2}^{1/2})^{3/4} \tag{5.57}$$

When oxygen partial pressure is relatively high, it is presumed that the hydrogen partial pressure is low giving the following assumption [32]:

$$K_{5.53}p_{H_2}^{1/2} = \frac{[OH_O^{\bullet}]}{[h^{\bullet}]} << 1 \tag{5.58}$$

which further means

$$[OH_O^{\bullet}] << [h^{\bullet}] \tag{5.59}$$

By using the assumption in Eq. 5.58, Eq. 5.56 is reduced to be

$$[V_M^{\prime\prime\prime}] = \frac{K_{5.22}^{1/8}}{3^{3/4}} \cdot p_{O_2}^{3/16} \tag{5.60}$$

This relation indicates that at relatively high oxygen partial pressure, the rate constant due to the metal vacancy is a function of the oxygen partial pressure only. Thus, varying water vapour content

in the atmosphere does not change the rate constant, which is congruent to the experimental results shown in Fig. 5.9.

However, in the case of relatively low oxygen partial pressure, the hydrogen partial pressure is presumed to be high giving the following assumption [32]:

$$K_{5.53} p_{H_2}^{1/2} = \frac{[OH_O^{\bullet}]}{[h^{\bullet}]} >> 1 \tag{5.61}$$

which means

$$[OH_O^{\bullet}] >> [h^{\bullet}] \tag{5.62}$$

By using the assumption in Eq. 5.61, Eq. 5.57 can be reduced to be

$$[V_M'''] = \frac{K_{5.22}^{1/8} K_{5.53}^{3/4} K_w^{3/8}}{3^{3/4}} \cdot p_{H_2O}^{3/8} \tag{5.63}$$

This relation indicates that at relatively low oxygen partial pressure, the defect concentration and therefore the parabolic rate constant increases with the increased water vapour content in the atmosphere. This analysis is in agreement with the experimental results in Figs. 5.10 (a) and (b). Nevertheless, this relation predicts that in this low oxygen partial pressure range the hydrogen partial pressure does not affect the rate constant, while the experimental results in Fig. 5.10(c) show that it does. In this case, the defect situation according to this model is probably oversimplified.

It is noted that when the assumptions according to Reaction 5.61 and 5.62 are applied, the electroneutrality condition according to Eq. 5.55 reduces to be $3[V_M'''] = [OH_O^{\bullet}]$. Furthermore, the $OH_O^{\bullet}$ formation reaction i.e. Reaction 5.53 stems from the $H_i^{\bullet}$ formation reaction i.e. Reaction 5.27 and therefore the dependency of these two defect concentrations on gas pressure are in the same form. As a result, the relationship of the metal vacancy and gas pressure according to Eq. 5.63 is equivalent to that derived from the case III where $3[V_M'''] = [OH_O^{\bullet}]$ and metal vacancy is dominant, i.e. Eq. 5.48 in Section 5.3.2.

Hänsel et al. [32] further considered the possibility that the metal interstitial ($M_i^{\bullet\bullet\bullet}$) is a dominant defect. As described in Reaction 1.25 in Chapter 1, the defect reaction for M_2O_3 formation in the present case may be written as follows:

$$\frac{3}{2}O_2 + 2M_i^{\bullet\bullet\bullet} + 6e' \leftrightarrow 2M_M + 3O_O \tag{5.64}$$

with the equilibrium constant of

$$K_{5.64} = \frac{1}{[M_i^{\bullet\bullet\bullet}]^2 [e']^6 p_{O_2}^{3/2}} \tag{5.65}$$

They also proposed that in the region near the metal/scale interface, the formation of negatively charged hydrogen interstitial might be possible by the following reaction:

$$\frac{1}{2}H_2 + e' \leftrightarrow H_i' \tag{5.66}$$

with the equilibrium constant of

$$K_{5.66} = \frac{[H_i']}{[e'] p_{H_2}^{1/2}} \tag{5.67}$$

The charge balance condition in this case is

$$3[M_i^{\bullet\bullet\bullet}] = [e'] + [H_i'] \tag{5.68}$$

From Eqs. 5.65, 5.67 and 5.68, it can be obtained that

$$[M_i^{\bullet\bullet\bullet}] = \left(\frac{1}{3^{3/4} K_{5.64}^{1/8}} \right) \cdot \frac{1}{p_{O_2}^{3/16}} \cdot (1 + K_{5.66} p_{H_2}^{1/2})^{3/4} \tag{5.69}$$

From Eqs. 5.69 and 5.2, it can be obtained that

$$[M_i^{\bullet\bullet\bullet}] = \left(\frac{1}{3^{3/4} K_{5.64}^{1/8} K_w^{3/8}} \right) \cdot \frac{p_{H_2}^{3/8}}{p_{H_2O}^{3/8}} \cdot (1 + K_{5.66} p_{H_2}^{1/2})^{3/4} \tag{5.70}$$

In the case when the oxygen partial pressure is relatively low, we may consider that the hydrogen partial pressure is relatively high leading to the following assumption [32]:

$$K_{5.66} p_{H_2}^{1/2} = \frac{[H_i']}{[e']} >> 1 \tag{5.71}$$

which also means

$$[H_i'] >> [e'] \tag{5.72}$$

From the assumption in Eq. 5.71, Eqs. 5.69 and 5.70 are reduced to be

$$[M_i^{\bullet\bullet\bullet}] = \left(\frac{K_{5.66}^{3/4}}{3^{3/4} K_{5.64}^{1/8}} \right) \cdot \frac{p_{H_2}^{3/8}}{p_{O_2}^{3/16}} = \left(\frac{K_{5.66}^{3/4}}{3^{3/4} K_{5.64}^{1/8} K_w^{3/8}} \right) \cdot \frac{p_{H_2}^{3/4}}{p_{H_2O}^{3/8}} \tag{5.73}$$

This relation shows that, in the low oxygen partial pressure range, the defect concentration and therefore the rate constant increase with the increased hydrogen partial pressure at constant oxygen partial pressure. The prediction according to Eq. 5.73 is in agreement with the experimental result in Fig. 5.10(c), while the one according to Eq. 5.63 is not. However, this relation fails to explain the experimental results in Fig. 5.10(b) which shows that the rate constant increases with water vapour at the fixed hydrogen partial pressure.

From the analysis in this section, it was summarised [27, 32] that no single defect model can be used to explain the oxidation mechanism in the atmosphere containing water vapour. However, the linear combination of the mass-transfer contributions by metal vacancy and metal interstitials according to Eqs. 5.56 and 5.69 together with the equilibrium of the hydrogen dissolution reaction i.e. Reaction 5.74, contains all relations between the rate constant and the gas partial pressure at the low oxygen partial pressure regime [27, 32].

$$H_2 + O_O \leftrightarrow OH_O^{\bullet} + H_i' \tag{5.74}$$

5.3.4 Effect of Hydroxyl Ion on the Oxygen Transport in the Oxide

Sections 5.3.2 and 5.3.3 consider the possibility that hydrogen interstitial is formed and might be bounded with the oxygen in the oxide giving the substitutional hydroxyl ion, $OH_O^{\bullet}$. Thereafter, this defect affects the defect structure of the oxide, such as increasing the metal vacancy concentration in

the condition that water vapour content is high, thus contributing to the increased oxidation rate. However, the hydroxyl ion could also directly affect the diffusion of oxygen in the oxide as suggested by Galerie [8, 37].

Again in the classic 2001 paper, Galerie et al. [8] suggested that hydrogen from water vapour could be incorporated into the oxide by jumping into the substitutional site usually occupied by O^{2-} or into the oxide grain boundary. The species stemed from water vapour that can jump into the substitutional site are the adsorbed OH ($OH-s$) or H^+ which might form the substitional hydroxyl by the following reactions [8]:

$$OH-s+V_O^{\bullet\bullet}+e' \rightarrow OH_O^{\bullet} \tag{5.75}$$

$$H^+ + O_O \rightarrow OH_O^{\bullet} \tag{5.76}$$

For the lattice transport, the oxygen vacancy is needed for the diffusion of $OH_O^{\bullet}$ [8]. Wouters et al. [38] discussed that the ionic radius of the hydroxyl ion (OH^-) is about 90 pm while that of oxygen ion (O^{2-}) is about 140 pm, and the charge of OH^- is also less than that of O^{2-}. It is then expected that the diffusion coefficient of the hydroxyl ion through vacancies is higher than that of the oxygen ion [38]. For the transport along the grain boundary, the charge of the diffusing species must go along with the semiconducting property of the oxide, i.e. the p-type metal-deficient oxide allows the anion transport and the n-type oxygen-deficient oxide allows the cation transport [8].

For thermally grown chromia on chromium and stainless steels, the photoelectrochemistry measurement showed that the semiconducting type of the oxide turned from amphoteric p+n when oxidised in oxygen into n when oxidised in water vapour [37, 39]. This effect is less for stainless steel since the iron doping into the oxide might weaken its p-type property [37, 39]. From these results, we may consider that, for the oxidation of chromium or the chromia-forming stainless steel in water vapour, the hydroxyl ion might be incorporated into the oxide in the substitutional site and diffuses via the oxygen vacancy, or it might be incorporated into the oxide grain boundary and further diffuses to the metal/scale interface. Bamba et al. [37, 40] oxidised Fe–15Cr–0.5Si in Ar-10% H_2O at 850 ºC and found the presence of OH in the oxide. Furthermore, Chandra-ambhorn et al. [5, 37] oxidised AISI 441 and AISI 444 stainless steels in O_2 and H_2-2% H_2O at 800 ºC and took these samples to assess the scale adhesion using the tensile test as explained in Section 2.3 in Chapter 2. They found that the oxide formed in H_2-2% H_2O is better adhered to the steel substrate [5] as shown in Fig. 6.4 in Chapter 6. The similar trend was also observed for the thermal scale on Fe–15.7Cr–8.5Mn formed in humidified oxygen compared with the one formed in oxygen [33]. The better adhesion indicates the possibility that the hydroxyl ion diffuses inwardly to form oxide at the metal/scale interface and therefore promotes the scale adhesion.

5.4 Characteristics of the Scale Formed in Humidified Atmosphere

Section 5.3 reviews the defect structure in M_2O_3 formed in water vapour. It represents the simple case of chromia which is a major oxide thermally grown on stainless steel. However, in the real case of stainless steel, the situation is more complex since the other oxides can also be formed and water vapour can also affect the other properties of the metal-scale system. These aspects will be reviewed in the present section.

Issartel et al. [41] reported the oxidation mechanism of 4509 ferritic steel (Fe–18Cr–Nb–Ti) at 1000 ºC in air-7.5% H_2O. They presented that, under water-containing oxidising condition, chromia and Cr–Mn spinel with the composition of $Mn_{1.5}Cr_{1.5}O_4$ were formed while chromium species volatilisation occurs simultaneously. The oxidant, H^+ and/or H_2O, inwardly transported through oxide scale and reacted not only with chromium to form chromia but also with iron at the chromium-depleted zone to form wüstite (FeO). Chromia internally formed owing to chromium oxidation meanwhile it was consumed by reacting with FeO to form $FeCr_2O_4$. FeO could possibly react with H_2O which diffuses internally through scale and forms Fe_3O_4. At the same time, iron

outwardly diffused and externally reacted with H_2O and Fe_2O_3 is then formed as a nodule which was a sign of catastrophic or breakaway oxidation.

Many works reported that the catastrophic oxidation of stainless steels occurs by the formation of Fe-rich nodules (haematite nodules) on the top surface [41–43]. Breakaway is highly dependent on the partial pressure of water vapour [44]. In the presence of water vapour, the breakaway can be reached faster than that in dry condition that means water vapour accelerates the onset of breakaway oxidation kinetics [45, 46]. There are many researches describing how Fe-rich nodule grows. As the increasing of scaling growth rate, the thicker scale is formed on the alloy exposed to wet condition rather than to dry condition. So, the cracks and spallation occur faster than that exposed to dry condition. Since the cracks occur, Fe_2O_3 could be thermodynamically reproduced and this oxide is indeed observed to grow [39]. Ehlers et al. [47] pointed out that the transformation of protective chromia into non-protective iron-rich oxide is governed by the ratio of H_2O/O_2 rather than the absolute level of H_2O. The competitive adsorptions of H_2O and O_2 at the metal surface governs whether breakaway oxidation occurs [47]. Therefore, the occurrence of breakaway oxidation is determined by H_2O/O_2 ratio and it was found experimentally that a critical condition for breakaway is $p_{H_2O} / p_{O_2} > 1$ [47].

The breakaway oxidation can also be enhanced by other effects like the chromium species volatilisation and acidity of the surface. Segerdahl et al. [48] oxidised 11% Cr steel (CrMoV11 1) in dry and wet O_2 with the humidity of 10% or 40 % at the temperature range of 450–700 ºC. In wet atmosphere, either protective oxide or non-protective oxide was formed on the steel while chromium species volatilisation occurred in both cases. The oxide formed on the steels remains protective whenever the chromium loss by volatilisation and chromium supply by solid state diffusion to the oxide are still balance. If the rate of chromium loss is higher than the chromium-supplying rate, the oxide transforms from protective internal chromium-rich $(Cr,Fe)_2O_3$ and external iron-rich $(Cr,Fe)_2O_3$ to non-protective internal $(Fe,Cr)_3O_4$ and α-Fe_2O_3 due to the depletion of chromium resulting in the feasibility of breakaway oxidation. In addition, the presence of water vapour is more corrosive to alloy comparing with dry atmosphere by promoting higher chromium species volatilisation rate, and then the breakaway oxidation is reached. As for the acidity of the oxide surface, due to more acidity of Fe_2O_3 than Cr_2O_3, when Fe_2O_3 grows on the existing Cr_2O_3, the difference of surface acidities of these oxides arises, so the faster catastrophic oxidation occurs [43]. In order to prolong the lifetime of alloys, sufficient chromium must be presented in the alloy for selectively oxidising and forming a protective chromia scale. If alloyed chromium is not enough, iron-rich nodule, rather than the desired chromia, co-exists on the alloys [49].

Water vapour cannot only lead to the catastrophic oxidation, it can also change the properties of the oxide-metal system. Chromium exposed to water-containing atmosphere tends to internally oxidise more than that exposed to dry condition due to hydrogen dissolved in alloys [46, 50, 51]. This may affect one or more following factors: oxygen solubility, oxygen diffusivity in alloys, alloy interdiffusion coefficient and parabolic rate constant [51]. Ani et al. [52] also described that, even though the dissolved hydrogen does not influence the diffusion coefficient of chromium, it increases the oxygen permeability in α-Fe in wet condition by a factor of 1.4 comparing with that in dry condition. This results in the increase in minimum concentration of chromium to form an external scale. Additionally, the dissolved hydrogen changes the oxide shape from discrete spherical particle in dry atmosphere to spike-like precipitates leading to the enhancement of oxygen transport along the metal/oxide precipitate interface [52]. Although many studies reported that water vapour extensively affects the scaling rate of oxide, it is rather different from the recent research by Cheng et al. [53] indicating that water vapour accelerated the formation of oxide scale but it was not significant. The difference in water vapour percentage does not affect the composition of the scale. However, water vapour causes the oxide grain refinement comparing with the oxide formed in dry condition which is consistent with the works of Othman et al. [49] and Jacob et al. [54].

For alumina-forming alloys, many researches confirmed that water vapour had little effect on their oxidation kinetics whenever the α-alumina was extensively formed on the alloy surface

[55–58]. However, according to the study of Janakiraman et al. [59] demonstrating the cyclic oxidation of PWA 1480, PWA 1484, CMSX 4, diffusion aluminide coatings on PWA 1480 and PWA 1484, and Co–24Cr–10.5Al–0.3Y in wet and dry atmospheres at 1100 ºC, it was found that, in cases that alumina scale was cracked and spalled in dry air, the presence of water vapour caused the increasing in degradation rate by a factor of 2. On the contrary, if there was no crack or spallation of alumina in dry air, water vapour had no effect on the oxidation behaviour. Furthermore, it was proposed that water vapour caused stress corrosion cracking at alumina/alloy interface during cyclic oxidation.

Nevertheless, there is a research proved that water vapour affects the early stage oxidation of alumina-forming alloy. Götlind et al. [60] isothermally oxidised FeCrAl alloy Kanthal AF at 900 ºC in dry O_2 and O_2-40% H_2O. They found that the oxidation rate was significantly faster in wet atmosphere than in dry one during the first 72 h. The development of alumina in dry and wet O_2 at 900 ºC was proposed to be as follows: stage (1), γ-Al_2O_3 and the mixture of oxides corresponding to the composition of the alloy nucleate on the surface. After prolonged exposure, a chromium-rich band within the alumina scale is observed. At stage (2), γ-Al_2O_3 outwardly grows with the high rate leading to rapid mass gain. Also, γ-Al_2O_3 provides outward mass transport paths for divalent cations. Meanwhile, α-Al_2O_3 nucleates and grows slowly inwards and laterally. Pores form in γ-Al_2O_3 layer close to the inner oxide interface. After 1 h of exposure, the size and distribution of the pores are essentially the same in dry and wet O_2. Then, stage (3), a continuous layer of inward-growing α-Al_2O_3 forms. This layer restricts the supply of cations for the growth of outer γ-Al_2O_3 layer resulting in a much slower oxidation rate. After that, the mechanisms in dry and wet oxidations are different. In dry O_2, the outer oxide changes into a mixture oxide phases resulting in the cease of outward oxide growth in which the α-Al_2O_3 is formed as the outer layer. The γ-Al_2O_3 continues its slow outward growth leading to the formation of an uneven oxide while the porosity decreases. The slower oxidation in dry O_2 is due to an increase in the effective thickness of the α-Al_2O_3 layer by transformation of γ-Al_2O_3 and by pore filling. On the other hand, in wet O_2, γ-Al_2O_3 does not transform to α-Al_2O_3 due to the stabilisation of γ-Al_2O_3 by H_2O forming a hydroxylate surface. The pores have no sign to disappear and the scale formed in wet condition is thicker than that formed in dry condition. This makes an alloy exposed to wet atmosphere more susceptible to spallation than that exposed to dry atmosphere.

5.5 Summary

This chapter reviews the role of water vapour on the high temperature corrosion of stainless steels, starting from the scenario when water vapour is in the bulk gas to the situation when it is at the solid/gas interface and in the oxide.

When water vapour is in the bulk gas, it can be dissociated giving oxygen and hydrogen. The oxygen uptake for oxidation of metals is not mainly from the oxygen dissociated from water vapour but from the water molecule itself. The dissociation of water can change the ratio of the partial pressure of water vapour to the partial pressure of hydrogen (p_{H_2O} / p_{H_2}), which could further affect the stability of the oxide formed. The variation of this ratio when the oxidation kinetics are linear and parabolic is derived.

Once water vapour adsorbs on the surface, it can oxidise the metal or volatilise the formed oxide. In the case that water vapour cannot significantly enter the oxide and change its transport properties, the surface reaction especially the dissociation of the adsorbed OH to the adsorbed O can be a rate determining step. In that case, the more acidic oxide, as indicated by the less negative value of the cation hydration enthalpy, tends to have the faster linear oxidation rate. The surface reaction-controlled kinetics cannot be observed in the chromium oxidation in water vapour but can be found when stainless steel is oxidised in carbon-containing atmosphere.

Water vapour can also volatilise the chromia to the volatile species. The volatilisation rate depends on parameters such as the linear velocity of the gas in the atmosphere. At relatively slow

linear velocity, the volatilisation rate increases with the velocity, indicating that the rate is controlled by the mass transfer of the volatile species from the solid/gas interface to the bulk gas. When the velocity is higher, the volatilisation rate can be constant which indicates that the rate is controlled by the surface reaction. Coating or surface modification e.g. the pre-oxidation technique can be used to reduce the rate of chromium species volatilisation.

Many works reported that water vapour can be incorporated into the oxide primarily in the form of hydrogen interstitial with positively unit effective charge ($H_i^{\bullet}$). Based on Norby's work [35], the construction of the Brouwer diagram of M_2O_3 formed in humidified oxygen is derived, and the graphical representation of the role of water vapour on metal and oxygen vacancies concentrations is proposed. In the regime of relatively high water vapour, increasing water vapour increases the metal vacancy concentration which could contribute to the increased rate of the formation of the metal-deficient oxide. $H_i^{\bullet}$ can also be bounded with the oxygen in the oxide resulting in the substitutional hydroxyl defect ($OH_O^{\bullet}$). The hydrogen dissociation may also give $OH_O^{\bullet}$ and H_i'. The linear combination of the mass transfer due to metal vacancy and metal interstitial together with the hydrogen dissociation giving of the hydrogen defects ($OH_O^{\bullet}$ and H_i') were proposed by Hänsel et al. [32] to describe the defect situation in the chromia formed in water vapour. The hydroxyl ion could also help facilitate the inward oxygen transport due to its smaller ionic radius and charge compared with those of O^{2-}. For the chromia formed in water vapour, the oxide is found to be n-type and in this case the hydroxyl ion may transport via the oxygen vacancy or along the oxide grain boundary to the metal/oxide interface. The improved adhesion of scale on stainless steel formed in the atmosphere containing water vapour supports the possibility of this hydroxyl ion inward diffusion.

Apart from chromia, other oxides can be formed during the oxidation of stainless steel in water vapour and in many cases can lead to the catastrophic oxidation. This breakaway oxidation relates to many effects such as the p_{H_2O} / p_{H_2}. The chromium species volatilisaion or high acidity of the oxide can also provoke the breakaway oxidation. Water vapour can also affect the other properties of stainless steel or the oxide scale. It can increase the oxygen permeability in the ferrite matrix or refine the oxide grain boundaries. For the alumina-forming alloys, many works reported that water vapour has little effect on the oxidation kinetics. However, water vapour can affect the oxide formation on the alumina-forming stainless steel. It can stabilise the γ-alumina and form a thick and porous oxide leading to susceptibility to the oxide spallation.

References

[1] S.R.J. Saunders, M. Monteiro, F. Rizzo, The oxidation behaviour of metals and alloys at high temperatures in atmospheres containing water vapour: A review, Prog. Mater. Sci. 53 (2008) 775–837.

[2] W.F. Quadakkers, F. Żurek, Oxidation in steam and steam/hydrogen environments, in: R.A. Cottis, M.J. Graham, R. Lindsay, S.B. Lyon, J.A. Richardson, J.D. Scantlebury, F.H. Stott (Eds.), Shreir's Corrosion, forth ed., Elsevier, The Netherlands, 2010, pp. 407–456.

[3] S. Chandra-ambhorn, K. Ngamkham, N. Jiratthanakul, Effects of process parameters on mechanical adhesion of thermal oxide scales on hot-rolled low carbon steels, Oxid. Met. 80 (2013) 61–72.

[4] S. Chandra-ambhorn, T. Nilsonthi, Y. Wouters, A. Galerie, Oxidation of simulated recycled steels with 0.23 and 1.03 wt.% Si in Ar-20% H_2O at 900 ºC, Corros. Sci. 87 (2014) 101–110.

[5] S. Chandra-ambhorn, Y. Wouters, L. Antoni, F. Toscan, A. Galerie, Adhesion of oxide scales grown on ferritic stainless steels in solid oxide fuel cells temperature and atmosphere conditions, J. Power Sources 171 (2007) 688–695.

[6] W. Wongpromrat, H. Thaikan, W. Chandra-ambhorn, S. Chandra-ambhorn, Chromium vaporisation from AISI 441 stainless steel oxidised in humidified oxygen, Oxid. Met. 79 (2013) 529–540.

[7] W. Wongpromrat, G. Berthomé, V. Parry, S. Chandra-ambhorn, W. Chandra-ambhorn, C. Pascal, A. Galerie, Y. Wouters, Reduction of chromium volatilisation from stainless steel interconnector of solid oxide electrochemical devices by controlled preoxidation, Corros. Sci. 106 (2016) 172–178.

[8] A. Galerie, Y. Wouters, M. Caillet, The kinetic behaviour of metals in water vapour at high temperatures: can general rules be proposed?, Mater. Sci. Forum 369-372 (2001) 231–238.

[9] O. Kubaschewski, E.LL. Evans, Metallurgical Thermochemistry, third ed. (reprinted), Pergamon, Great Britain, 1965.

[10] M. Ueda, Communication during seminar at Tokyo Institute of Technology, 2015.

[11] D. Caplan, M. Cohen, The volatilization of chromium oxide, J. Electrochem. Soc. 108 (1961) 438–442.

[12] R.T. Grimley, R.P. Burns, M.G. Inghram, Thermodynamics of the vaporization of Cr_2O_3: dissociation energies of CrO, CrO_2, and CrO_3, J. Chem. Phys. 34 (1961) 664–667.

[13] C.S. Tedmon, The effect of oxide volatilization on the oxidation kinetics of Cr and Fe–Cr alloys, J. Electrochem. Soc. 113 (1966) 766–768.

[14] C.A. Stearns, F.J. Kohl, G.C. Fryburg, Oxidative vaporization kinetics of Cr_2O_3 in oxygen from 1000º to 1300 ºC, J. Electrochem. Soc. 121 (1974) 945–951.

[15] G.C. Fryburg, R.A. Miller, F.J. Kohl, C.A. Stearns, Volatile products in the corrosion of Cr, Mo, Ti, and four superalloys exposed to O_2 containing H_2O and gaseous NaCl, J. Electrochem. Soc. 124 (1977) 1738–1743.

[16] H. Asteman, J.-E. Svensson, L.-G. Johansson, M. Norell, Indication of chromium oxide hydroxide evaporation during oxidation of 304L at 873 K in the presence of 10% water vapor, Oxid. Met. 52 (1999) 95–111.

[17] H. Asteman, J.-E. Svensson, M. Norell, L.-G. Johansson, Influence of water vapor and flow rate on the high-temperature oxidation of 304L; effect of chromium oxide hydroxide evaporation, Oxid. Met. 54 (2000) 11–26.

[18] H. Asteman, J.-E. Svensson, L.-G. Johansson, Evidence for chromium evaporation influencing the oxidation of 304L: the effect of temperature and flow rate, Oxid. Met. 57 (2002) 193–216.

[19] H. Asteman, J.-E. Svensson, L.-G. Johansson, Oxidation of 310 steel in H_2O/O_2 mixtures at 600 ºC: the effect of water-vapour-enhanced chromium evaporation, Corros. Sci. 44 (2002) 2635–2649.

[20] A. Yamauchi, K. Kurokawa, H. Takahashi, Evaporation of Cr_2O_3 in atmospheres containing H_2O, Oxid. Met. 59 (2003) 517–527.

[21] C. Gindorf, L. Singheiser, K. Hilpert, Vaporisation of chromia in humid air, J. Phys. Chem. Solids 66 (2005) 384–387.

[22] E.J. Opila, D.L. Myers, N.S. Jacobson, I.M.B. Nielsen, D.F. Johnson, J.K. Olminsky, M.D. Allendorf, Theoretical and experimental investigation of the thermochemistry of $CrO_2(OH)_{2(g)}$, J. Phys. Chem. A 111 (2007) 1971–1980.

[23] H. Kurokawa, C.P. Jacobson, L.C. De Jonghe, S.J. Visco, Chromium vaporization of bare and of coated iron–chromium alloys at 1073 K, Solid State Ionics 178 (2007) 287–296.

[24] M. Stanislowski, E. Wessel, K. Hilpert, T. Markus, L. Singheiser, Chromium vaporization from high-temperature alloys I. chromia-forming steels and the influence of outer oxide layers, J. Electrochem. Soc. 154 (2007) A295–A306.

[25] D.J. Young, B.A. Pint, Chromium volatilization rates from Cr_2O_3 scales into flowing gases containing water vapor, Oxid. Met. 66 (2006) 137–153.

[26] R.B. Bird, W.E. Stewart, E.N. Lightfoot, Transport Phenomena, second ed., John Wiley & Sons, USA, 2002.

[27] D.J. Young, High Temperature Oxidation and Corrosion of Metals, second ed., Elsevier, The Netherlands, 2016.

[28] P. Promdirek, G. Lothongkum, S. Chandra-ambhorn, Y. Wouters, A. Galerie, Oxidation kinetics of AISI 441 ferritic stainless steel at high temperatures in CO_2 atmosphere, Oxid. Met. 81 (2014) 315–329.

[29] P. Promdirek, G. Lothongkum, S. Chandra-ambhorn, Y. Wouters, A. Galerie, Behaviour of ferritic stainless steels subjected to dry gas atmospheres at high temperatures, Mater. Corros. 62 (2011) 616–622.

[30] P. Promdirek, G. Lothongkum, Y. Wouters, S. Chandra-ambhorn, A. Galerie, Effect of humidity on the corrosion kinetics of ferritic stainless steels subjected to synthetic biogas, Mater. Sci. Forum 696 (2011) 417–422.

[31] S. Chandra-ambhorn, A. Jutilarptavorn, T. Rojhirunsakool, High temperature oxidation of irons without and with 0.06 wt.% Sn in dry and humidified oxygen, Corros. Sci. 148 (2019) 355–365.

[32] M. Hänsel, W.J. Quadakkers, D.J. Young, Role of water vapor in chromia-scale growth at low oxygen partial pressure, Oxid. Met. 59 (2003) 285–301.

[33] S. Chandra-ambhorn, P. Saranyachot, T. Thublaor, High temperature oxidation behaviour of Fe–15.7 wt.% Cr–8.5 wt.% Mn in oxygen without and with water vapour at 700 ºC, Corros. Sci. 148 (2019) 39–47.

[34] W. Zhang, B. Hua, J. Yang, B. Chi, J. Pu, L. Jian, Performance evaluation of a new Fe–Cr–Mn alloy in the reducing atmosphere of solid oxide fuel cells, J. Alloys Compd. 769 (2018) 866–872.

[35] T. Norby, Protonic defects in oxides and their possible role in high temperature oxidation, J. Phys. IV Colloque 3 (1993) 99–106.

[36] B. Tveten, G. Hultquist, T. Norby, Hydrogen in chromium: influence on the high-temperature oxidation kinetics in O_2, oxide-growth mechanisms, and scale adherence, Oxid. Met. 51 (1999) 221–233.

[37] A. Galerie, M.R. Ardigo, P. Berthod, W. Chandra-ambhorn, S. Chevalier, P.Y. Hou, F. Rouillard, Chapter1 Influence of water vapour on high-temperature oxidation of chromia-forming materials, in: S. Chevalier, J. Favergeon (Eds.), French Activity on high temperature corrosion in water vapor, Trans tech publications, Switzerland, 2014, pp. 1–25.

[38] Y. Wouters, A. Galerie, J.-P. Petit, Thermal oxidation of titanium by water vapour, Solid State Ionics 104 (1997) 89–96.

[39] A. Galerie, J.-P. Petit, Y. Wouters, J. Mougin, A. Srisrual, P.-Y. Hou, Water vapour effects on the oxidation of chromia-forming alloys, Mater. Sci. Forum 696 (2011) 200–205.

[40] G. Bamba, Y. Wouters, A. Galerie, G. Borchardt, S. Shimada, O. Heintz, S. Chevalier, Inverse growth transport in thermal chromia scales on Fe–15Cr steels in oxygen and in water vapour and its effect on scale adhesion, Scr. Mater. 57 (2007) 671–674.

[41] C. Issartel, H. Buscail, Y. Wang, R. Rolland, M. Vilasi, L. Aranda, Water vapour effect on ferritic 4509 steel oxidation between 800 and 1000 ºC, Oxid. Met. 76 (2011) 127–147.

[42] S. Henry, Influence de la vapeur d'eau sur l'oxydation à haute température du chrome et de quelques aciers inoxydables ferritiques stabilisées, PhD Thesis, Institut National Polytechnique de Grenoble, France, 2000.

[43] A. Galerie, S. Henry, Y. Wouters, M. Mermoux, J.-P. Petit, L. Antoni, Mechanisms of chromia scale failure during the course of 15–18Cr ferritic stainless steel oxidation in water vapour, Mater. High Temp. 21 (2005) 105–112.

[44] A. Galerie, Y. Wouters , M. Pijolat, F. Valdivieso, M. Soustelle, T. Magnin, D. Delafosse, C. Bosch, B. Bayle, Mechanisms of corrosion and oxidation of metals and alloys, Adv. Eng. Mater. 3 (2001) 555–561.

[45] S. Henry, A. Galerie, L. Antoni, Abnormal oxidation of stabilized ferritic stainless steels in water vapor, Mater. Sci. Forum 369-372 (2001) 353–360.

[46] N.K. Othman, N. Othman, J. Zhang, D.J. Young, Effects of water vapour on isothermal oxidation of chromia-forming alloys in Ar/O_2 and Ar/H_2 atmospheres, Corros. Sci. 51 (2009) 3039–3049.

[47] J. Ehlers, D.J. Young, E.J. Smaardijk, A.K. Tyagi, H.J. Penkalla, L. Singheiser, W.J. Quadakkers, Enhanced oxidation of the 9%Cr steel P91 in water vapour containing environments, Corros. Sci. 48 (2006) 3428–3454.

[48] K. Segerdahl, J.-E. Svensson, M. Halvarsson, I. Panas, L.-G. Johansson, Breakdown of the protective oxide on 11% Cr steel at high temperature in the presence of water vapor and oxygen, the influence of chromium vaporization, Mater. High Temp. 21 (2005) 69–78.

[49] N.K. Othman, J. Zhang, D.J. Young, Water vapour effects on Fe–Cr alloy oxidation, Oxid. Met. 73 (2010) 337–352.

[50] E. Essuman, G.H. Meier, J. Żurek, M. Hänsel, W.J. Quadakkers, The effect of water vapor on selective oxidation of Fe–Cr alloys, Oxid. Met. 69 (2008)143–162.

[51] E. Essuman, G.H. Meier, J. Żurek, M. Hänsel, L. Singheiser, W.J. Quadakkers, Enhanced internal oxidation as trigger for breakaway oxidation of Fe–Cr alloys in gases containing water vapor, Scr. Mater. 57 (2007) 845–848.

[52] M.H.B. Ani, T. Kodama, M. Ueda, K. Kawamura, T. Maruyama, The effect of water vapor on high temperature oxidation of Fe-Cr alloys at 1073 K, Mater. Trans. 50 (2009) 2656–2663.

[53] X. Cheng, Z. Jiang, D. Wei, L. Hao, J. Zhao, J. Peng, S. Lu, L. Jiang, Effect of water vapor on oxidation of ferritic stainless steel 21Cr-0.6Mo-Nb-Ti in simulated reheating environment, Adv. Mater. Res. 690–693 (2013) 280–289.

[54] Y.P. Jacob, V.A.C. Haanappel, M.F. Stroosnijder, H. Buscail, P. Fielitz, G. Borchardt, The effect of gas composition on the isothermal oxidation behaviour of PM chromium, Corros. Sci. 44 (2002) 2027–2039.

[55] I. Kvernes, M. Oliveira, P. Kofstad, High temperature oxidation of Fe–13Cr–*x*Al alloys in air/H_2O vapour mixtures, Corros. Sci. 17 (1977) 237–252.

[56] T. Åkermark, G. Hultquist, Oxygen exchange in oxidation of an Fe–20Cr–10Al alloy in ~10 mbar O_2/H_2O-gas mixtures at 920 ºC, Oxid. Met. 47 (1997) 117–137.

[57] Z. Liu, T. Narita, Oxidation behavior of TiAl(Cr, Ag) at 900 ºC in water vapor, Intermetallics 12 (2004) 459–468.

[58] K. Onal, M.C. Maris-Sida, G.H. Meier, F.S. Pettit, Water vapor effects on the cyclic oxidation resistance of alumina forming alloys, Mater. High Temp. 20 (2003) 327–337.

[59] R. Janakiraman, G.H. Meier, F.S. Pettit,The effect of water vapor on the oxidation of alloys that develop alumina scales for protection, Metall. Mater. Trans. A 30 (1999) 2905–2913.

[60] H. Götlind, F. Liu, J.-E. Svensson, M. Halvarsson, L.-G. Johansson, The effect of water vapor on the initial stages of oxidation of the FeCrAl alloy Kanthal AF at 900 ºC, Oxid. Met. 67 (2007) 251–266.